

Comparison of seasonal and spatial variations of albedos from Moderate-Resolution Imaging Spectroradiometer (MODIS) and Common Land Model

L. Zhou,¹ R. E. Dickinson,¹ Y. Tian,¹ X. Zeng,² Y. Dai,¹ Z.-L. Yang,³ C. B. Schaaf,⁴ F. Gao,⁴ Y. Jin,⁴ A. Strahler,⁴ R. B. Myneni,⁴ H. Yu,¹ W. Wu,¹ and M. Shaikh¹

Received 17 December 2002; revised 24 April 2003; accepted 2 May 2003; published 15 August 2003.

[1] This paper compares seasonal and spatial variations of Moderate Resolution Imaging Spectroradiometer (MODIS) albedos with those from the Common Land Model (CLM) by land cover type. MODIS albedo data in the year 2001 were used to determine seasonal, spatial, and land cover dependence at 1 km resolution and to investigate the biases in CLM. Albedo dependence on vegetation type is smaller than that on snow and soil. Snow causes the largest temporal and spatial variations, especially in the visible band (0.3–0.7 μm). CLM has visible albedos that are lower by up to 0.4–0.5 in winter over northern high latitudes but are globally higher by 0.02–0.04 in summer over most vegetation, mainly due to its overestimated leaf and stem area index in winter and slightly higher prescribed canopy albedos in summer, respectively. MODIS and CLM differ considerably in soil albedo over desert and semidesert regions, especially in the near-infrared band (0.7–5.0 μm), with the largest low bias of about 0.1 in the Sahara. Adjustments of the prescribed albedos in CLM based on MODIS observations could reduce such biases. Therefore the model should better represent leaf and stem area index, vegetation albedo in the presence of snow, and soil albedo.

INDEX TERMS: 1620 Global Change: Climate dynamics (3309); 1640 Global Change: Remote sensing; 3307 Meteorology and Atmospheric Dynamics: Boundary layer processes; 3322 Meteorology and Atmospheric Dynamics: Land/atmosphere interactions; *KEYWORDS:* albedo, MODIS, Common Land Model, leaf area index

Citation: Zhou, L., et al., Comparison of seasonal and spatial variations of albedos from Moderate-Resolution Imaging Spectroradiometer (MODIS) and Common Land Model, *J. Geophys. Res.*, 108(D15), 4488, doi:10.1029/2002JD003326, 2003.

1. Introduction

[2] The land surface and its ecosystems play an important role in determining exchanges of energy, momentum, water, heat, carbon dioxide, and other greenhouse gases between the land surface and the atmosphere [Dickinson, 1983; Sellers et al., 1997]. Land surface processes have been characterized in climate models by parameterizations that range from rather simple schemes to complex representations. Key model parameters include albedo, fractional vegetation and snow cover, roughness length, surface skin temperature, and canopy properties [Dickinson et al., 1993; Bonan, 1996; Sellers et al., 1996]. However, these variables have been only crudely represented due to limited observations. Satellites provide information of global spatial sampling at regular temporal intervals and thus have the capability to estimate

accurately model parameters globally. The availability of satellite observations has motivated many modelers to improve the representation of interactions between soil, vegetation, and the atmosphere [Henderson-Sellers and Wilson, 1983; Buermann et al., 2001; Zeng et al., 2002].

[3] Albedo is the fraction of incident solar energy reflected by the land surface in all directions and determines how much radiation is absorbed by the surface. It changes as surfaces change, depending not only on the amount of vegetation cover but also on the surface texture and structure. A positive snow/ice-albedo feedback within the global climate system has been recognized [Rohbock, 1983; Intergovernmental Panel on Climate Change, 2002]. Higher albedos due to desertification and deforestation result in a reduction of precipitation and evapotranspiration [Dickinson and Henderson-Seller, 1988; Xue et al., 1990; Xue and Shukla, 1993; Hahmann and Dickinson, 1997]. Bonan [1998] suggests that high soil albedos over the Sahara desert in the NCAR Community Climate Model version 3 (CCM3) may generate land surface air temperatures that are several degrees colder than observations throughout the year. Evidently, inaccuracy or errors in specification of surface albedo in climate models may result in other such serious biases.

[4] Albedo in climate models is represented by processes rather than by simple tables of numbers. Hence satellite observations can be best used to validate and improve

¹School of Earth and Atmospheric Sciences, Georgia Institute of Technology, Atlanta, Georgia, USA.

²Institute of Atmospheric Physics, University of Arizona, Tucson, Arizona, USA.

³Department of Geological Sciences, University of Texas at Austin, Austin, Texas, USA.

⁴Department of Geography, Boston University, Boston, Massachusetts, USA.

model parameterizations. *Wei et al.* [2001] compared albedos of two land surface models (LSMs), the biosphere-atmosphere transfer scheme (BATS), and the NCAR LSM, with those derived from remote-sensed data. Both BATS and LSM demonstrated a large bias over snow covered, desert and semidesert regions. Consequently, *Zeng et al.* [2002] adjusted albedo parameterizations in the Common Land Model (CLM) coupled with CCM3 and found a significant reduction in the summer cold bias over desert and semidesert regions.

[5] Further comparison using new satellite data and in situ measurements is necessary. The albedo data by *Wei et al.* [2001] were derived from Advanced Very High Resolution Radiometers (AVHRRs), whose quality may be degraded by atmospheric effects, satellite drift, and changeover [*Gutman, 1999*]. *Privette et al.* [1997] demonstrate that sparse angular samples from AVHRR may result in poor albedo retrievals. *Wei et al.* [2001] focused only on comparison of total albedos over a broad spectral band (0.3–5.0 μm). Here we address albedos as used in climate models, composed of visible (<0.7 μm) and near-infrared (>0.7 μm) spectral bands, each with diffuse and direct components. Such comparison based on detailed spectral bands may be more helpful in finding reasons for large biases in models. Furthermore, *Wei et al.* [2001] used satellite albedo data from only 2 months. Here we more carefully examine the seasonal cycle of albedo.

[6] High-quality albedo products from the Moderate Resolution Imaging Spectroradiometer (MODIS) are now publicly released [*Schaaf et al., 2002*]. This paper compares seasonally and spatially MODIS albedos in the year 2001 with those from CLM and investigates possible reasons for major biases. It considers how this information may be used to improve albedo parameterizations in CLM. Section 2 describes how surface albedo is computed from CLM and MODIS. Section 3 analyzes seasonal and spatial variations of MODIS albedos in 2001 at 1 km resolution. Differences of coarse resolution albedo between CLM and MODIS are compared and possible reasons are discussed in section 4. Section 5 concludes the major results.

2. Albedo From CLM and MODIS

2.1. MODIS Albedo

[7] Remotely sensed surface albedos are generated from empirical and semiempirical models. The MODIS albedo algorithm adopts a semiempirical, kernel-driven linear Bidirectional Reflectance Distribution Function (BRDF) model to characterize the anisotropy of the global surface [*Lucht et al., 2000a*]. The BRDF model relies on the weighted sum of three parameters that are retrieved from the multivariate multiangular cloud-free atmospherically corrected surface reflectances at 1 km resolution acquired by MODIS in a 16-day period. The algorithm uses only the snowy observations to make a retrieval if the majority of days in a 16-day period have been snow covered, otherwise a snow-free BRDF retrieval is made [*Schaaf et al., 2002*]. By integrating the retrieved BRDF models over all viewing angles, seven spectral albedos can be obtained. Three broadband (0.3–0.7, 0.7–5.0, and 0.3–5.0 μm) albedos were also obtained through spectral to broadband conversions [*Liang et al., 1999; Liang, 2001*].

[8] The MODIS albedos represent the best quality retrieval possible over each 16-day period, and quality assurance value (QA) fields are attached to the data. We can use the QA data to tell whether the data are from snow or nonsnow pixels or are of good quality (i.e., data with sufficient high-quality input surface reflectances and well distributed over the viewing hemisphere that result in a well-fit model). For those cases where a full retrieval is not possible due to insufficient or poor sampling or a poor fit, albedos are retrieved from a backup method using available observations to adjust a priori knowledge of archetypal surface BRDFs [*Strugnell et al., 2001*].

[9] The MODIS albedo products provide a standard suite of global black- and white-sky albedos in an integerized sinusoidal grid projection with tiles representing 1200 pixels on the Earth. Black-sky albedo (directional hemispherical reflectance) represents the direct beam contribution while white-sky (bihemispherical reflectance) refers to the entire diffuse contribution. Actual albedos can be derived from a linear combination of white- and black-sky albedos, depending on the fraction of diffuse skylight (MODIS BRDF/Albedo Product (MOD43B) User's Guide, <http://geography.bu.edu/brdf/userguide/albedo.html>).

[10] Here we used the local noon black-sky albedo product (MOD43B3, validated version V003) in 2001 for the visible (VIS, 0.3–0.7 μm) and near-infrared (NIR, 0.7–5.0 μm) bands with periods starting at Julian dates of 1, 17, 33, 49, 65, 81, 97, 113, 129, 145, 193, 209, 225, 241, 257, 273, 289, 305, 321, 337, and 353. Periods starting at days 161 and 177 are missing due to sensor breakdown. White-sky albedos behave similarly to black-sky albedos at local solar noon and are not shown separately here.

2.2. CLM Albedo

[11] Model albedos were produced from CLM coupled with NCAR CCM3. CCM3 is a spectral atmospheric model with resolution at about $2.8^\circ \times 2.8^\circ$ and 18 vertical levels [*Kiehl et al., 1998*]. CLM is a recently developed state-of-the-art LSM, described in detail by *Zeng et al.* [2002] and *Dai et al.* [2003]. CLM has 1 vegetation layer, 10 unevenly spaced vertical soil layers, and up to 5 snow layers. Every surface grid (about $2.8^\circ \times 2.8^\circ$) is subdivided into up to five tiles and each tile contains a single land cover type. *Zeng et al.* [2002] used 16 land cover types (Table 1) based on IGBP land cover classification and defined a special class type 18 (purely bare soil). Surface input data required for each grid include central location, soil color type, percentage of sand and clay of soil, and land cover type and fraction for each tile. Each vegetation type is assigned a set of time-invariant parameters: optical properties (canopy albedo), morphological properties (canopy roughness, canopy zero plane displacement, inverse square root of leaf dimension, and root fraction), and physiological properties. Time-variant parameters include leaf area index (LAI) and stem area index (SAI).

[12] Albedo at each grid is calculated from that of three components: bare soil, snow, and vegetation,

$$\alpha = \alpha_s f_s + \alpha_{sn} f_{sn} + \alpha_v f_v, \quad (1)$$

where α stands for albedo, f stands for fraction, and the subscripts, s , sn , and v refer to bare soil, snow, and vegeta-

Table 1. Land Cover Types Used in CLM

Class	Land Cover Types
1	evergreen needleleaf forests
2	evergreen broadleaf forests
3	deciduous needleleaf forests
4	deciduous broadleaf forests
5	mixed forests
6	closed shrublands
7	open shrublands
8	woody savannas
9	savannas
10	grasslands
11	permanent wetlands
12	croplands
13	urban and built-up lands
14	cropland/natural vegetation mosaics
15	snow and ice
16	barren or sparsely vegetated
18 ^a	purely bare soil

^aA special class defined as land cover type 18 in CLM.

tion, respectively. Note $f_s + f_{sn} + f_v = 1$. The two components in α_{sn} are snow covered soil and snow covered vegetation, therefore f_{sn} is a sum of the fraction of snow covered soil, f_{scs} , and vegetation, f_{scv} , given by

$$f_{scs} = z_{snow} / (10z_g + z_{snow}), \quad (2)$$

$$f_{scv} = z_{snow} / (10z_v + z_{snow}). \quad (3)$$

z_{snow} is snow depth in meters, z_g and z_v are bare soil and vegetation roughness, respectively.

2.2.1. Bare Soil Albedo

[13] The α_s varies with soil color and soil moisture, calculated from

$$\alpha_s = \alpha_{sat} + \min\{\alpha_{sat}, \max[0.01(11 - 40\theta), 0]\}, \quad (4)$$

where α_{sat} is the albedo for saturated soil, θ is the ratio of surface soil water volumetric content over its saturated value. Note dependence of soil albedo on solar zenith angle (SZA) is ignored. CLM uses eight soil color types from dark to light. The prescribed values for α_{sat} are given in Table 2a.

2.2.2. Snow Albedo

[14] The α_{sn} depends on SZA and snow age, and how the latter decreases with time due to growth of snow grain size and accumulation of dirt and soot [Wiscombe and Warren, 1980]. The treatment of snow albedo in CLM is directly adopted from BATS. The α_{sn} consists of direct beam albedo α_{snb} and diffuse albedo α_{snd} ,

$$\alpha_{snb} = \alpha_{snd} + 0.4f(\mu)[1 - \alpha_{snd}], \quad (5)$$

$$\alpha_{snd} = [1 - \phi F_{AGE}] \alpha_{sn0}, \quad (6)$$

where ϕ is a constant (CLM sets $\phi = 0.2$ for VIS and 0.5 for NIR), α_{sn0} is the new snow albedo at $SZA \leq 60^\circ$ (CLM sets $\alpha_{sn0} = 0.95$ for VIS and 0.65 for NIR), μ is cosine of SZA, and $f(\mu)$ is a factor between 0 and 1 used to increase snow albedo for $SZA > 60^\circ$,

$$f(\mu) = \begin{cases} \frac{1}{2} \left[\frac{3}{1+4\mu} - 1 \right], & \text{if } \mu \leq 0.5 \\ 0, & \text{if } \mu > 0.5 \end{cases} \quad (7)$$

F_{AGE} denotes the fractional reduction of snow albedo due to snow aging (assumed to represent increasing grain size and soot) for $SZA \leq 60^\circ$,

$$F_{AGE} = \frac{\tau_{snow}}{1 + \tau_{snow}}, \quad (8)$$

where τ_{snow} is a nondimensional snow age, incremented as a model prognostic variable,

$$\Delta\tau_{snow} = 1 \times 10^{-6}(r_1 + r_2 + r_3)\Delta t, \quad (9)$$

where Δt is the model time step. The term r_1 represents the effect of grain growth due to vapor diffusion, the temperature dependence being essentially proportional to the vapor pressure of water:

$$r_1 = \exp\left[5000\left(\frac{1}{273.16} - \frac{1}{T_{g1}}\right)\right], \quad (10)$$

where T_{g1} denotes surface soil temperature. The term r_2 represents the additional effect near and at freezing of meltwater,

$$r_2 = \min[r_1^{10}, 1], \quad (11)$$

and the term r_3 represents the effect of dirt and soot (CLM sets $r_3 = 0.01$ over Antarctica and 0.3 elsewhere).

2.2.3. Vegetation Albedo

[15] The α_v is calculated by a simplified two-stream scheme. This scheme assumes vegetation is homogeneous and combines canopy and its underlying surface albedo to capture essential features. It ignores multiple scattering, as is reasonable for the visible spectra and green leaves. The α_v can be divided into direct beam albedo α_{vb} and diffuse albedo α_{vd} :

$$\alpha_{vb} = \alpha_c \left[1 - \exp\left(-\frac{\omega\beta L_{sai}}{\mu\alpha_c}\right) \right] + \alpha_g \exp\left[-\left(1 + \frac{0.5}{\mu}\right)L_{sai}\right], \quad (12)$$

$$\alpha_{vd} = \alpha_c \left[1 - \exp\left(-\frac{2\omega\beta L_{sai}}{\alpha_c}\right) \right] + \alpha_g \exp(-2L_{sai}), \quad (13)$$

where α_c and α_g are canopy and underlying surface albedos, respectively, $\omega\beta$ is the upward scattering fraction (CLM sets $\beta = 0.5$, $\omega = 0.15$ for VIS and 0.85 for NIR), and L_{sai} is leaf and stem area index (LSAI), $LSAI = LAI + SAI$.

Table 2a. CLM Parameters for Albedo for Different Colored Soils in Visible (0.3–0.7 μm) and Near-Infrared (0.7–5.0 μm)

Soil Color Type	Saturated Soil Albedo		Dry Soil Albedo	
	Visible	Near-Infrared	Visible	Near-Infrared
1	0.12	0.24	0.24	0.48
2	0.11	0.22	0.22	0.44
3	0.10	0.20	0.20	0.40
4	0.09	0.18	0.18	0.36
5	0.08	0.16	0.16	0.32
6	0.07	0.14	0.14	0.28
7	0.06	0.12	0.12	0.24
8	0.05	0.10	0.10	0.20

Table 2b. CLM Parameters for Canopy Albedo for IGBP Land Cover Types in Visible (0.3–0.7 μm) and Near-Infrared (0.7–5.0 μm)

Land Cover Type	Visible	Near-Infrared
1	0.04	0.20
2	0.04	0.20
3	0.05	0.23
4	0.07	0.24
5	0.06	0.24
6	0.07	0.26
7	0.14	0.32
8	0.06	0.21
9	0.07	0.26
10	0.07	0.25
11	0.06	0.18
12	0.06	0.24
13	0.06	0.22
14	0.06	0.22
15	0.95	0.65
16	0.19	0.38

[16] This scheme assumes that vegetation albedo approaches that of the underlying surface, α_g , when L_{sai} goes to zero and approaches prescribed canopy albedo values, α_c , when L_{sai} goes to its maximum value. These prescribed albedos for each land cover type (Table 2b) were initially from BATS and then adjusted based on analysis of AVHRR-derived albedo data [Zeng *et al.*, 2002]. Figure 1 shows α_{vb} as a function of L_{sai} for vegetation with canopy albedos, $\alpha_c = 0.04$ for VIS and 0.2 for NIR, under two underlying surface conditions at $\text{SZA} = 60^\circ$: (1) snow, $\alpha_g = 0.85$ for VIS and 0.5 for NIR and (2) bare soil, $\alpha_g = 0.1$ for VIS and 0.2 for NIR. The α_{vb} starts from α_g when $L_{\text{sai}} = 0$, changes quickly as L_{sai} increases from 0 to 1.5, and gradually approaches α_c when L_{sai} reaches 2.5. Evidently, vegetation albedo is very sensitive for $\text{LSAI} < 1$ and becomes saturated for $\text{LSAI} > 2.5$.

[17] An 11-year simulation of CLM with climatological sea surface temperatures (SSTs) coupled with CCM3

was performed. Albedos from the last year are used to compare with MODIS albedos while the first 10-year run is used as a spin-up. To make the comparison more precise, local noon VIS and NIR black-sky albedos in CLM were sampled each day and were then averaged over every 16-day period specified in the MODIS albedo data.

3. Seasonal and Spatial Variations of MODIS Albedo at 1 km Resolution

[18] We used the MODIS land cover product (MOD12Q1) [Friedl *et al.*, 2002], which supplies an IGBP land cover classification map, to spatially aggregate all 1 km MODIS pixels into 5° latitudinal bands by IGBP land cover type. Albedo mean and standard deviation (STD) were calculated for each land cover type. To minimize errors due to misclassification, for each land cover type, only those bands that contain more than 0.2% of all global pixels belonging to that land cover were used. Note that there are no albedo data over Antarctic and some data are missing over regions beyond 70°N .

[19] MODIS albedo exhibits spatial and temporal similarities among dense forests (classes 1–5) and short vegetation (classes 6–12). For simplicity, we only show the results for four typical classes: evergreen needleleaf forests (class 1), evergreen broadleaf forests (class 2), open shrublands (class 7), and barren or sparsely vegetated (class 16).

[20] Spatial variations of MODIS albedo from south to north in Northern Hemisphere (NH) winter (averages of periods starting at days of 33, 49, 65, 81, i.e., approximately the period February–March) and summer (averages of periods starting at days of 193, 209, 225, 241, i.e., approximately the period July–August) were analyzed. The late winter averaging period is used to stay away from midwinter when there is too little sun to provide much energy either for the land surface or for remote

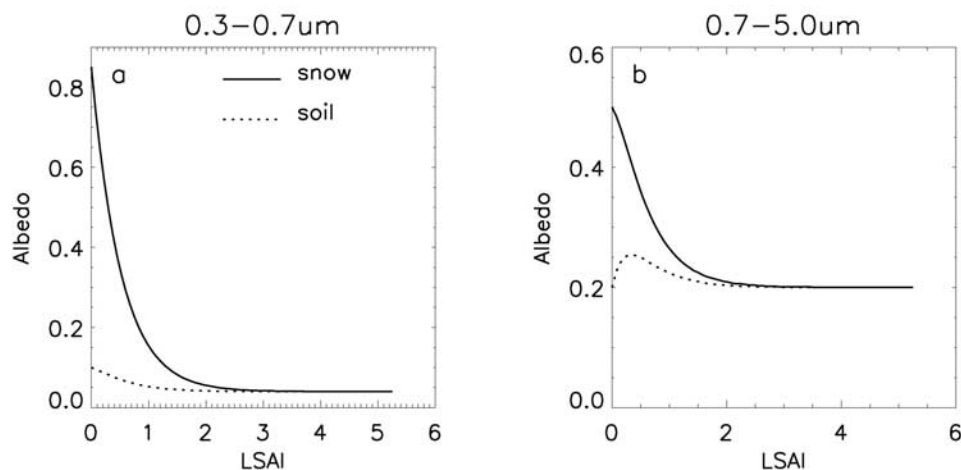


Figure 1. Vegetation albedo, α_{vb} , as a function of L_{sai} in equation (12) for vegetation with canopy albedos, $\alpha_c = 0.04$ in visible (VIS, 0.3–0.7 μm) and 0.20 in near-infrared (NIR, 0.7–5.0 μm), under two underlying surface conditions at $\text{SZA} = 60^\circ$: (1) snow, $\alpha_g = 0.85$ for VIS and 0.5 for NIR and (2) bare soil, $\alpha_g = 0.1$ for VIS and 0.2 for NIR. (a) VIS and (b) NIR.

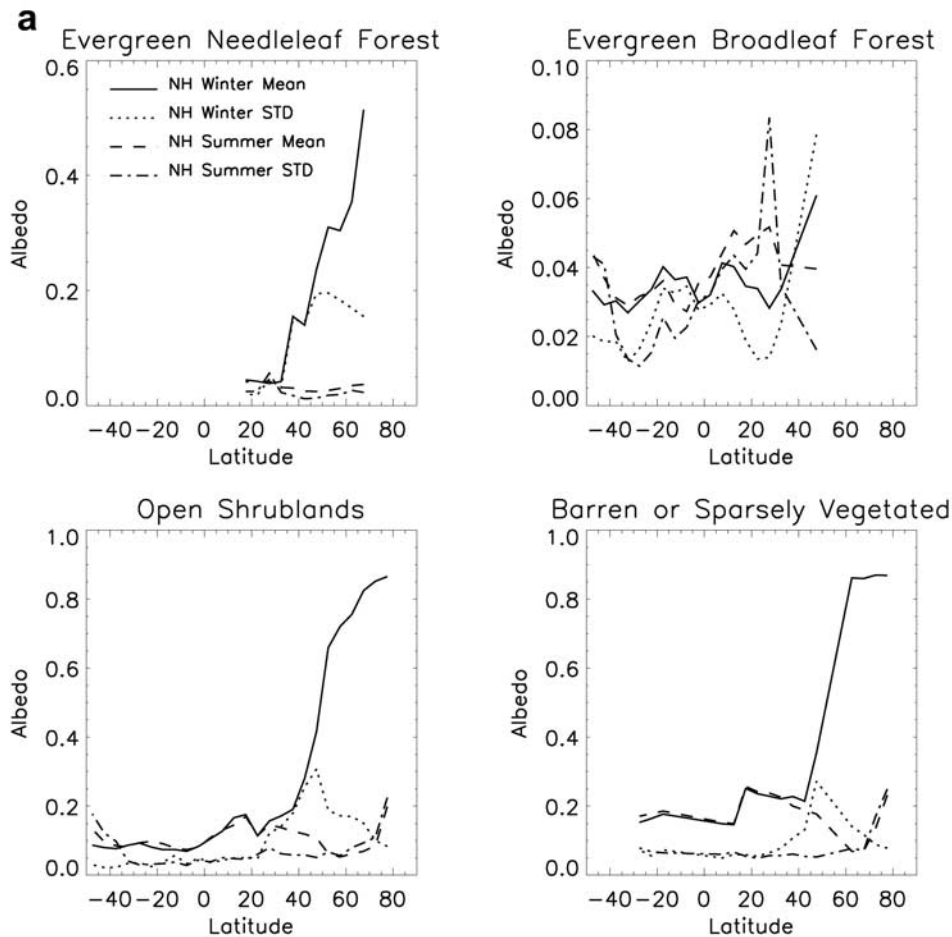


Figure 2. Spatial variations of MODIS albedo mean and standard deviation in winter and summer for evergreen needleleaf forests, evergreen broadleaf forests, open shrublands, and barren or sparsely vegetated, averaged over 1 km MODIS pixels: (a) VIS and (b) NIR.

sensing in high latitudes. The VIS albedo (Figure 2a) is extremely sensitive to the presence of snow. Albedo increases dramatically in winter but varies little during snow-free seasons from south to north. For example, the albedo around 70°N for class 1 varies from 0.04 in summer to 0.5 in winter. STD is the smallest over snow-free regions, maximizes around 50°N, where snow cover is partial, and declines in higher latitudes, where snow covers most of the ground. The NIR albedo (Figure 2b) shows similar variation to that of VIS but a less pronounced effect of snow, which only increases albedo by up to 0.2 from summer to winter. Apparently, snow results in the biggest spatial variations, several times larger than those due to differences in soil and land cover types. Variations in soil moisture and vegetation cover fraction results in the largest variations in snow-free albedo, especially for classes 7 and 16. Albedos for class 1 vary little due to little exposure of the underlying soil, while class 2 displays some variations associated with cloud contamination.

[21] Seasonal variations of MODIS albedo mean for four broad latitudinal bands, 50°N–70°N, 20°N–50°N, 20°S–20°N, and 20°S–50°S, were analyzed. The VIS albedo

(Figure 3a) increases dramatically from summer to winter for the bands 50°N–70°N and 20°N–50°N in the presence of snow. The further north the pixel, the larger and earlier the increase. Snow covers few pixels in the Southern Hemisphere (SH) and thus its effect is invisible from 20°S to 50°S. Albedos in 20°S–20°N display large variations for class 2 but vary little for class 16. The NIR albedo (Figure 3b) exhibits similar variation to that of VIS but the seasonal variations are much smaller even in high latitudes. Albedos in 50°N–70°N for classes 7 and 16 peak in early spring, consistent with the greatest accumulation of snowfall.

[22] We also used the MODIS QA data to analyze “good quality” pixels flagged with the mandatory good quality (=0). This flag reflects a full inversion and should show pixels of overall good quality. However, it is very conservative and some other good quality values may be missed. If there are not enough good quality pixels available for the statistics, pixels flagged with good quality (bits 0–3) in band 1 (red) were used since band 1 has stronger atmosphere effects than NIR. Results (not shown) indicate use of only the good quality pixels does not change the albedos shown in Figures 2 and 3 significantly except for class 2,

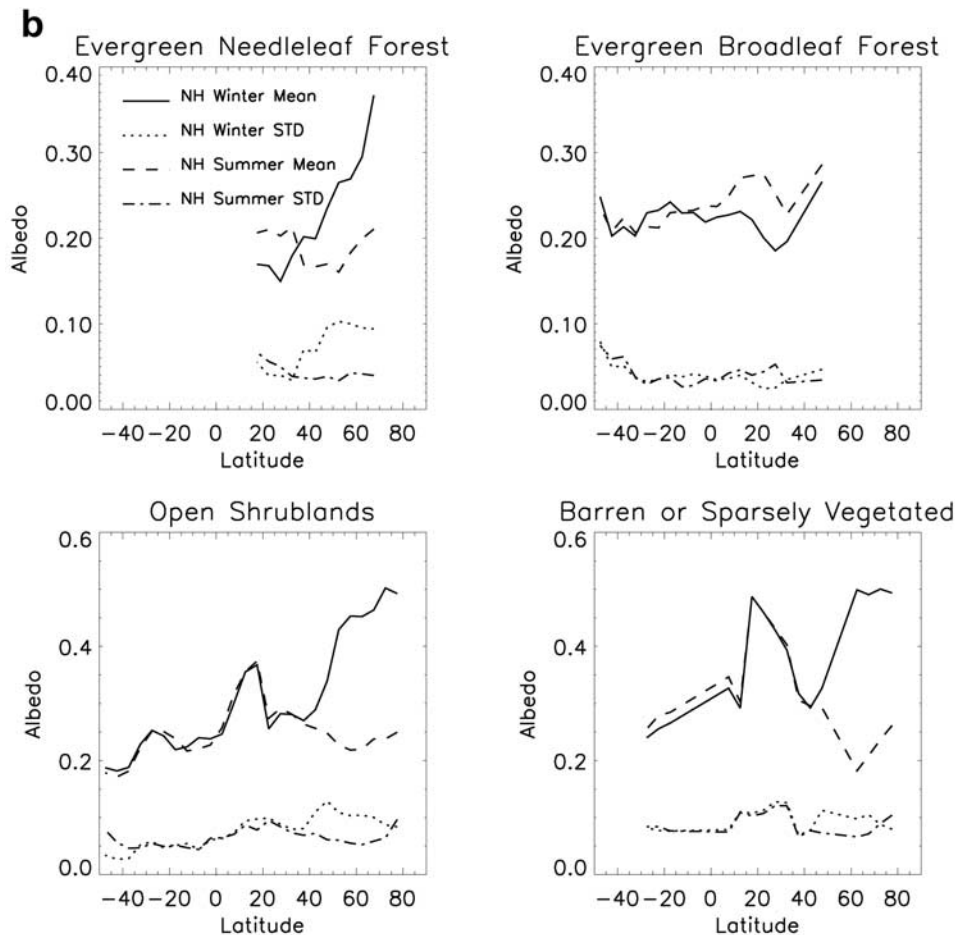


Figure 2. (continued)

which displays large variations of about 0.02 due to cloud contamination when all the data are used.

[23] Table 3 lists means and STDs of MODIS albedos by land cover type, averaged globally over periods starting at days of 193–214 in the NH and over periods starting at days of 17–65 in the SH when vegetation peaks. Albedos in the presence of snow differ significantly in their means and STDs within and among land cover types and thus are not listed. VIS albedos vary little in their means but have comparable STDs among vegetated land cover types, indicating large spatial variations within these vegetation types. Means and STDs in NIR albedo are about 0.2–0.27 and less than 0.08, respectively, for most land cover types. The albedo dependence on vegetation type is small compared to that on soil and snow. When the good quality pixels were used, albedo means and STD for all classes except class 15 (snow) tend to decrease. On average, VIS albedos are about 0.03 for dense forests and about 0.05–0.1 for short vegetation. Snow/ice and deserts show much high albedos.

[24] Table 3 can also be used to evaluate the accuracy of prescribed canopy albedos in CLM (Table 2b). Such comparison may provide the clues for reasons of large biases discussed in section 4. On average, most prescribed albedos in CLM are higher by 0.01–0.03 in VIS while differences in the NIR albedos are mixed. The largest differences are found for class 7 (open shrublands) in both VIS and NIR. Note here we are comparing the canopy albedos with those

from MODIS, which do not differentiate soil from vegetation at 1 km resolution. Consequently, the differences would be even larger, at least in VIS if canopy albedos were available from MODIS since soil albedo in VIS is generally larger than that for vegetation.

4. Comparison Between MODIS and CLM Albedos at Coarse Resolution

[25] In order to make a grid-by-grid comparison with CLM albedos, MODIS 1 km albedos were spatially aggregated to the CLM grids. The MODIS 1 km LAI [Myneni et al., 2002] in 2001 were processed similarly to evaluate the accuracy of LAI in CLM. Since the MODIS LAI main algorithm generally fails over snow covered pixels and the LAI values were generated with low confidence by the backup algorithm (W. Yang et al., Analysis of MODIS LAI and FPAR collections 1 and 3 data set time series from July 2000 to December 2002, submitted to *Remote Sensing of Environment*, 2003), only snow-free MODIS LAIs were used to exclude the influence of snow on LAI retrievals.

4.1. Spatial Pattern of Differences

[26] Global distributions for MODIS albedo and its differences from CLM were evaluated over every 16 days. For simplicity, only the results in NH winter and summer, defined in section 3, are shown (Figure 4). In general,

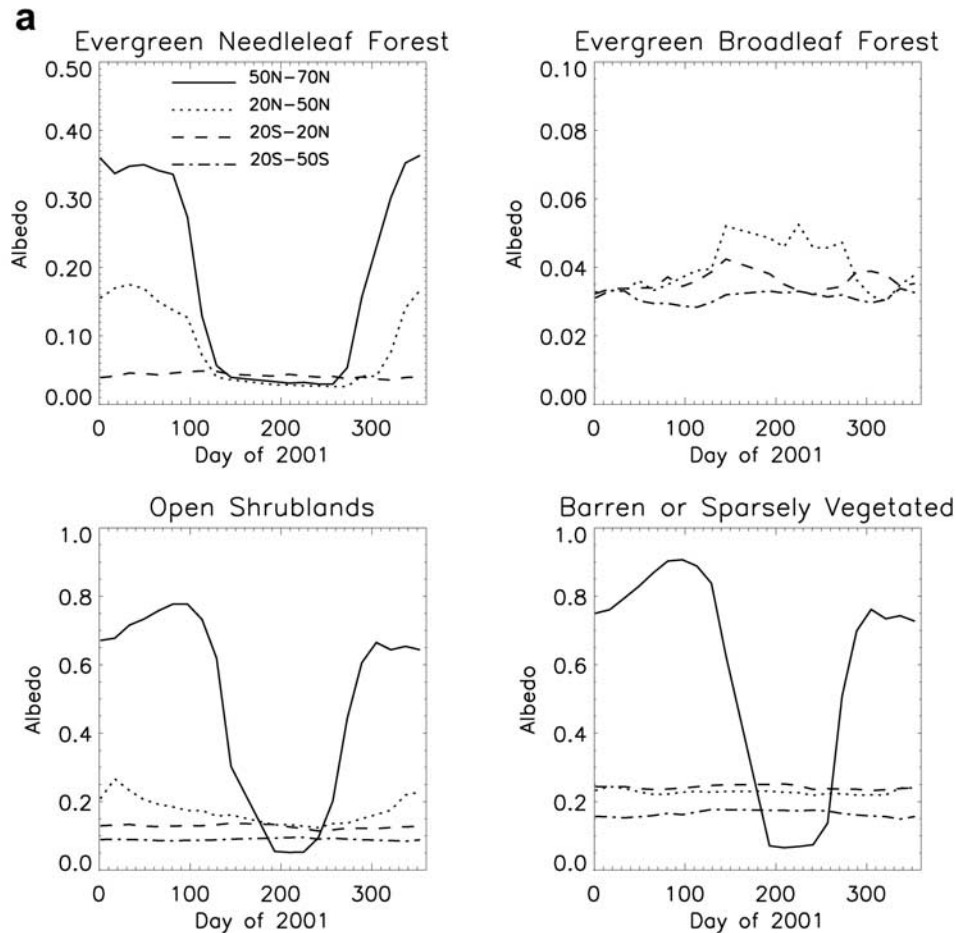


Figure 3. Seasonal variations of MODIS albedo means over four broad latitudinal bands, 50°N–70°N, 20°N–50°N, 20°S–20°N, and 20°S–50°S for evergreen needleleaf forests, evergreen broadleaf forests, open shrublands, and barren or sparsely vegetated, averaged over 1 km MODIS pixels: (a) VIS and (b) NIR. To minimize errors due to misclassification, for each land cover type, only those bands that contain more than 0.2% of all global pixels belonging to that land cover were used.

albedos of CLM are consistent with those of MODIS in spatial distribution and in rough agreement with the magnitude. Here we mainly focus on the notable differences.

[27] Compared to MODIS, CLM gives winter albedo lower by up to 0.4–0.5 and summer albedo higher by about 0.02–0.04 in VIS over northern high latitudes (Figures 4a and 4b). Albedos over deserts and semideserts in North Africa and the Arabian peninsula are underestimated by about 0.1 around the year, and the low bias could reach 0.2 over some regions. CLM overestimates albedos by about 0.02–0.04 over most regions in the SH.

[28] The situation is complex for the NIR albedo (Figures 4c and 4d). Both summer and winter albedos in CLM are (1) lower by up to 0.2 over the desert and semidesert region in North Africa and the Arabian peninsula, (2) higher by 0.02–0.1 over most regions in Australia, South America, and South Africa, and (3) lower by about 0.02 in the Amazon. We also see winter albedos higher by about 0.2 over Greenland and northern Canada. Elsewhere in Eurasia and North America, winter and summer differences are of both signs. Eastern US and Europe are predominantly higher in winter and lower in summer.

[29] Winter VIS and NIR albedos in CLM are higher by up to 0.5 and 0.3, respectively, over some regions in western China and neighboring areas (30°–50°N, 75°–100°E), while a small bias is seen over the same region for summer albedo.

4.2. Possible Reasons for the Spatial Differences

[30] Inaccurate or erroneous specification of albedo in CLM for soil, vegetation, or snow could cause the above mentioned albedo differences. To find possible reasons for such differences, we analyze seasonal and spatial variations of albedo, together with MODIS LAI and variables used to calculate model albedo: fraction of snow covered soil (f_{scs}), fraction of snow covered vegetation (f_{scv}), soil moisture (θ), LAI, SAI, snow depth, and snow age.

4.2.1. Snow-Related Albedo

[31] CLM is assigned pure snow albedos of 0.95 in VIS and 0.65 in NIR for $SZA \leq 60^\circ$ (Table 2b) derived from field measurements [Wiscombe and Warren, 1980]. MODIS gives pure snow albedo of 0.94–0.95 for VIS and 0.54–0.57 for NIR over Greenland. Hence MODIS has pure snow albedo, comparable in VIS but lower by about 0.1 in NIR than in CLM. Obviously, this disagree-

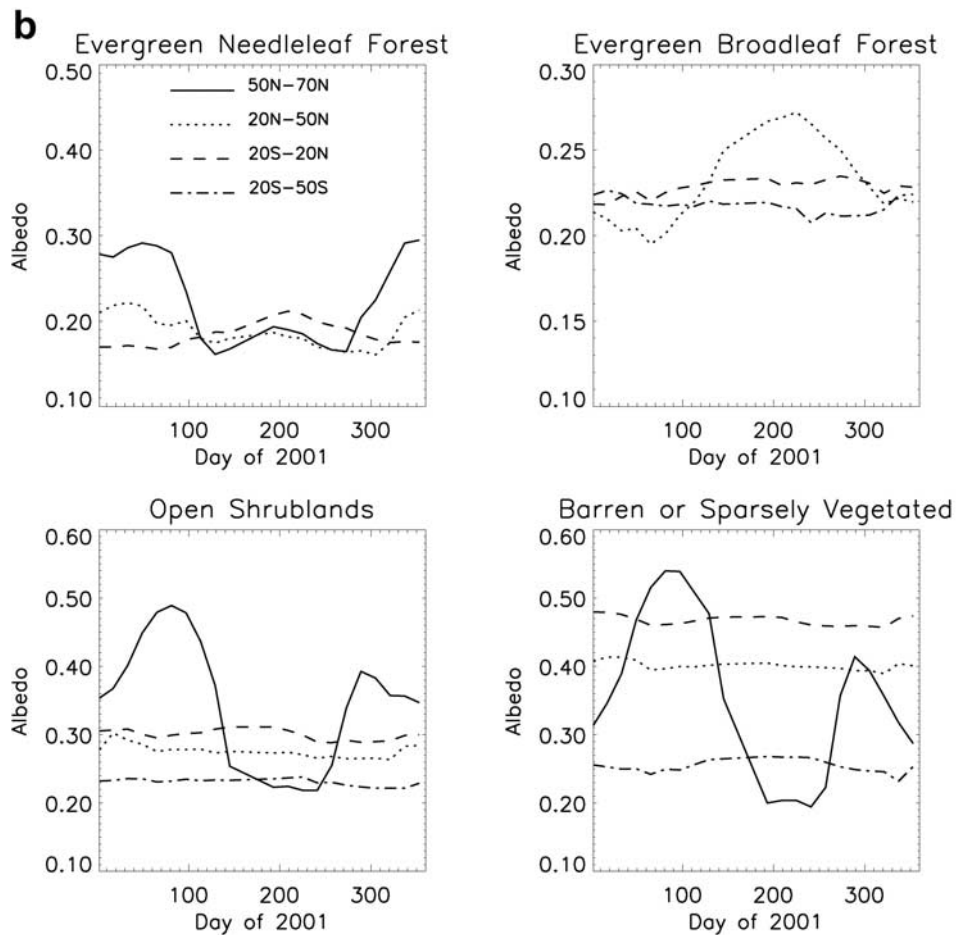


Figure 3. (continued)

ment can explain most of the albedo differences in NIR over Greenland but not the much lower albedos over most northern high latitudes (Figure 4). Part of the discrepancy could result from the presence of all sorts of shadowing,

leeds, ridges, etc. in the MODIS data that are not accounted for in CLM.

[32] The model could be wrong if it had the wrong snow cover. The issue can be discounted because most of the

Table 3. Spatial Average and Standard Deviation (STD) of MODIS 1 km Resolution Albedos Averaged Globally Over Periods Starting at Days of 193–214 in the Northern Hemisphere and Over Periods Starting at Days of 17–65 in the Southern Hemisphere for IGBP Land Cover Types

Land Cover Types	All Pixels			Pixels With High Quality		
	Visible	Near-Infrared	Pixel Numbers	Visible	Near-Infrared	Pixel Numbers ^a
1	0.03(0.02)	0.18(0.04)	7,024,498	0.03(0.01)	0.18(0.04)	4,050,410 (0.58)
2	0.04(0.03)	0.23(0.04)	15,598,634	0.03(0.01)	0.22(0.05)	388,508 (0.02)
2 ^b	0.03(0.02)	0.22(0.03)	8,928,450	0.03(0.01)	0.22(0.02)	4,324,209 (0.48)
3	0.03(0.01)	0.21(0.02)	2,366,488	0.03(0.01)	0.21(0.02)	1,723,750 (0.73)
4	0.03(0.03)	0.25(0.03)	1,958,996	0.03(0.01)	0.25(0.03)	662,016 (0.34)
5	0.03(0.02)	0.22(0.03)	8,104,106	0.03(0.01)	0.22(0.03)	4,786,686 (0.59)
6	0.06(0.03)	0.23(0.05)	1,022,966	0.05(0.02)	0.21(0.05)	234,759 (0.23)
7	0.10(0.06)	0.25(0.07)	31,527,380	0.10(0.05)	0.25(0.07)	11,998,813 (0.38)
8	0.04(0.02)	0.22(0.04)	9,833,413	0.04(0.02)	0.20(0.04)	1,804,521 (0.18)
9	0.05(0.03)	0.24(0.04)	10,352,324	0.05(0.02)	0.23(0.03)	955,986 (0.09)
10	0.09(0.04)	0.25(0.05)	12,014,283	0.09(0.04)	0.25(0.04)	6,339,295 (0.53)
11	0.04(0.02)	0.20(0.04)	530,810	0.04(0.02)	0.20(0.04)	343,518 (0.65)
12	0.06(0.03)	0.26(0.04)	14,557,552	0.05(0.01)	0.26(0.04)	6,099,820 (0.42)
13	0.06(0.03)	0.22(0.04)	260,617	0.05(0.02)	0.23(0.03)	79,857 (0.31)
14	0.05(0.02)	0.26(0.04)	5,265,418	0.04(0.01)	0.26(0.04)	1,472,264 (0.28)
15	0.81(0.24)	0.45(0.14)	2,483,496	0.88(0.16)	0.49(0.11)	1,992,766 (0.80)
16	0.22(0.07)	0.40(0.13)	21,806,138	0.22(0.06)	0.40(0.13)	15,372,802 (0.70)

^aValues in parenthesis represent percentage of high-quality pixels to total pixels.

^bAlbedos averaged globally over periods starting at days of 193–214 in the Southern Hemisphere in 0°S–15°S.

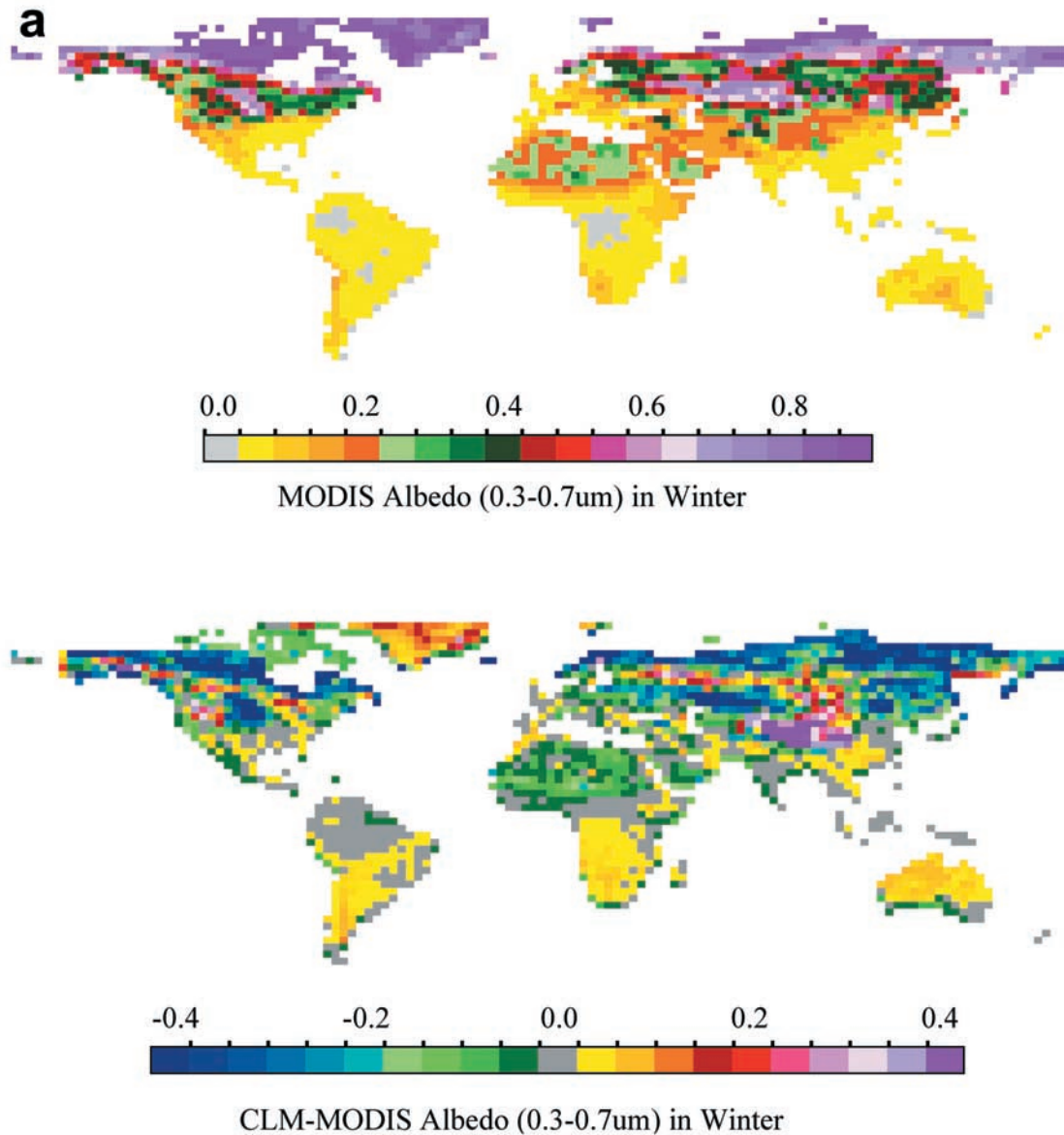


Figure 4. Spatial pattern of MODIS albedo and its difference from CLM (CLM-MODIS): (a) VIS in winter, (b) VIS in summer, (c) NIR in winter, and (d) NIR in summer.

largest biases are beyond 60°N, where snow covers about 70–100% of the bare soil. Snow albedo in CLM depends on SZA and snow age (equations (5) and (6)). In these regions, winter SZA is larger than 60°, which in fact increases model snow albedo, and snow age spatially varies little in CLM and could not contribute too much to the observed biases. Nor does snow-free soil albedo because 70–100% of the bare soil is covered by snow.

[33] Among the variables used to calculate model albedo, the LAI and SAI are tightly linked with the spatial pattern and magnitude of the albedo biases, especially over regions with large albedo biases. So CLM may overestimate LSAI and therefore mask snow too much. The presence of vegetation decreases snow albedo through (1) an increase in absorptance in VIS due to photosynthesis and (2) a reduction in openings exposed to sun and an increase in the fraction of shadow.

[34] Figure 5 shows the simulated albedo bias versus LSAI bias relation using equation (12) for three LSAI values: 0.2, 0.75, and 1.5. Parameters used include: (1) SZA = 60°; (2) canopy albedo, $\alpha_c = 0.05$ for VIS and 0.23 for NIR; and (3) underlying snow albedo, $\alpha_g = 0.85$ for VIS and 0.5 for NIR. An overestimation of 1.5 in LSAI results in an underestimation of 0.54 (0.21), 0.18 (0.10), and 0.04 (0.02) in VIS (NIR) albedo for the actual LSAI of 0.2, 0.75, and 1.5, respectively. Obviously, the albedo is more sensitive to the LSAI bias in VIS than in NIR.

[35] Table 4 lists area averages of winter albedo and LSAI beyond 50°N over model grids whose purity for the dominant land cover type is greater than 60%. As expected, VIS albedos show the largest bias, about 0.3 for short vegetation (classes 6, 7, 8, and 11) and 0.1–0.2 for needle-leaf forests (classes 1 and 3). NIR albedos have only small biases, due to the decreased sensitivity and lower NIR

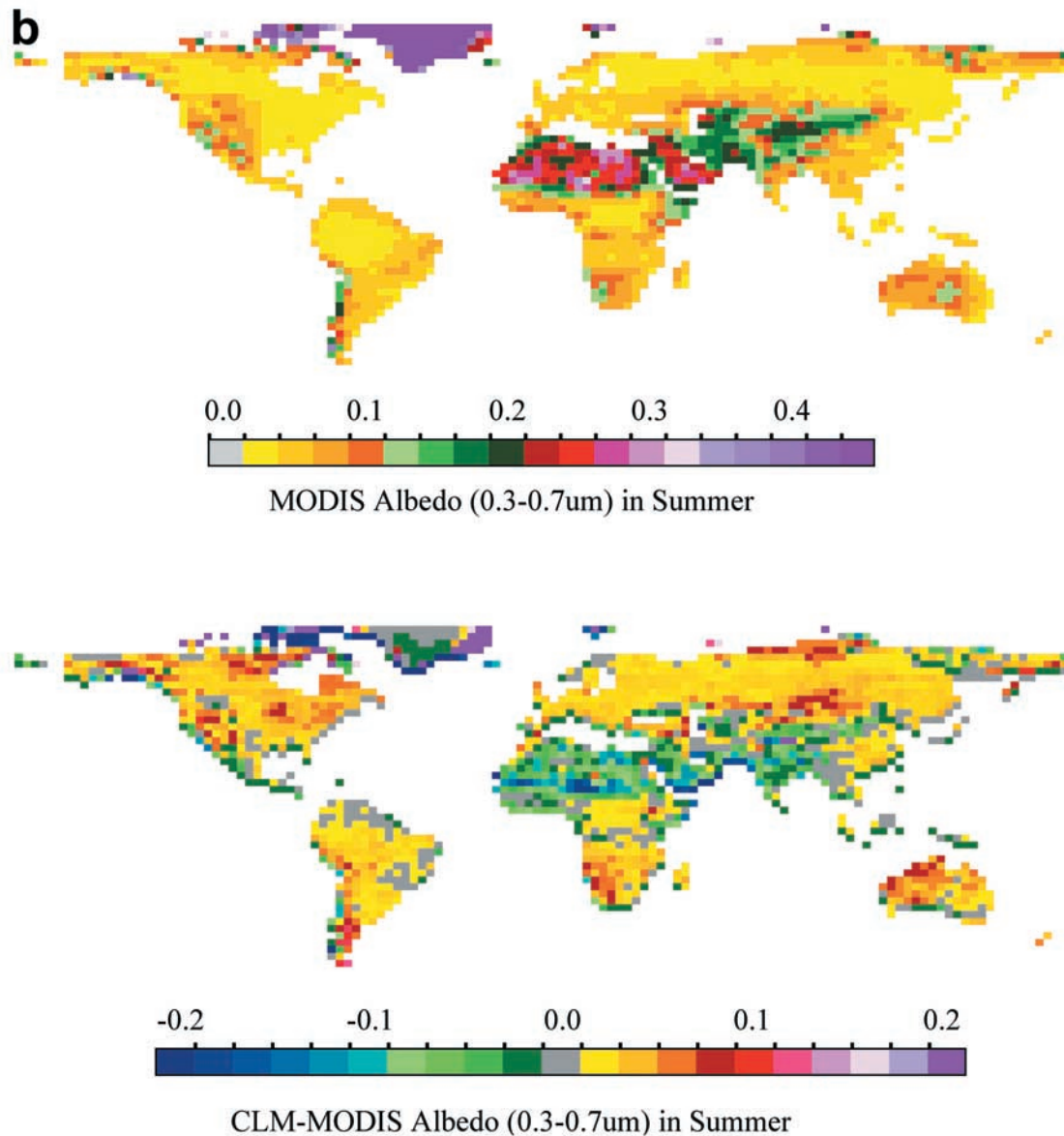


Figure 4. (continued)

albedos in MODIS than in CLM. The MODIS albedos except classes 12 and 14 differ little if only the snowy pixels are used due to few snow-free pixels available in these grids (based on the MODIS QA data). CLM has LSAIs about 1–2 for those classes, mainly from the SAI for short vegetation and LSAI for needleleaf forests. Note these values are averaged over grids and each class is not 100% pure.

[36] A model grid in Russia (63°N, 107°E) is used to illustrate seasonal variations of CLM and MODIS albedo (Figure 6). It consists of 75% deciduous needleleaf forests, 12% woody savannas, and 13% bare soil. In winter, snow covers more than 80% of the bare soil and about 5% of the vegetation. CLM with its LSAI of 1.1 has lower winter albedo than MODIS.

[37] CLM uses mean seasonal variations of LSAI for each IGBP land cover type within each 10° latitudinal zone. CLM LSAI assigns a “vegetated LSAI” for its “vegetated area” [Zeng *et al.*, 2002]. This means that the vegetated

LSAI is larger than the grid-averaged LSAI in Table 4. For example, the model is assigned vegetated LSAI of 3.3, 2.8, 1.2, and 1.4 for classes 1, 3, 7, and 8 in 60°N–70°N, respectively. With such high LSAIs in winter, α_v minimizes and approaches its prescribed canopy albedo (Figure 1). For a model grid dominated by vegetation, overestimated LSAI will underestimate its albedo. Evidently, for class 1, generally covering 80–90% of the model grids, LSAI of 3.3 results in a vegetation albedo of 0.04 in VIS, with the numerical value for grid albedo depending mainly on the small fraction of exposed snow.

[38] Figure 1 can be used to estimate approximately how much LSAI should be used in CLM to approach MODIS albedos in Table 4, assuming snow albedo starts at 0.84 (class 15). MODIS albedos of 0.4 for class 1 and 0.78 for class 7 correspond to LSAI values of 0.4 and 0.07, respectively. A short model test was run to see what CLM winter albedos would look like when these two LSAIs were used.

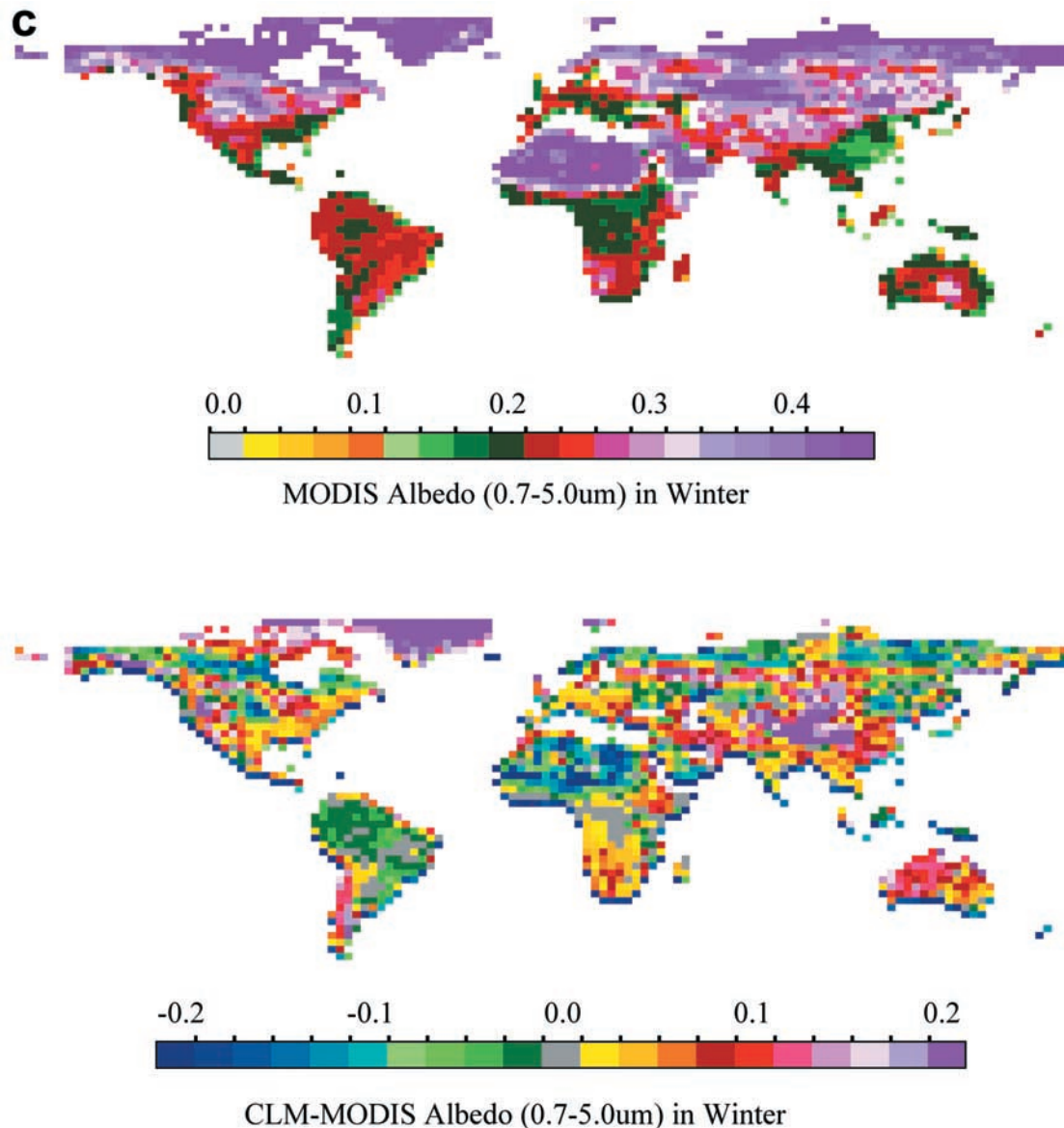


Figure 4. (continued)

Figure 7 (Figure 8) shows results for model grids only containing class 1 (class 7) beyond 50°N. Evidently, CLM significantly improves VIS albedo (Figures 7a and 8a), but overestimates NIR albedos (Figures 7b and 8b) due to the large difference of pure snow albedo in NIR between MODIS and model as previously discussed. When we simply set the model’s pure snow NIR albedo to the MODIS value of 0.49 (Table 3), as expected, CLM shows a notable improvement (Figures 7c and 8c).

[39] Thus the model albedo discrepancies may be largely explained by the model’s excess SAI for deciduous canopy and excess LSAI for needleleaf trees in winter. However, the above estimated LSAIs may be too small, especially for class 1, and part of the discrepancies may also result from inaccurate specifications of fractional vegetation cover, f_{scv} and f_{scs} in CLM (equations (2) and (3)). In addition, winter forest albedos from MODIS tend to be larger than those cited from in situ observations, possibly because more sunlit

gaps are observed by satellites than would field measurements made at low levels over the canopy [Jin *et al.*, 2002]. Snow over trees and snow/ice frozen on leaves may also have a contribution. At cold temperatures, needles may go dormant, and their accompanying compositional changes may change their spectral signal. Therefore simply “tuning” CLM LSAI to approach MODIS albedos may obscure deficiencies in representation of physical processes within the model.

[40] Evidently, CLM needs to better represent albedo for vegetation in the presence of snow. Snow enhances albedo in three ways: (1) sits in openings exposed to sun, (2) sits under the canopy, and (3) sits on the branches. CLM does not include snow on branches as a contribution to albedo; snow may fall or melt off soon after snowfall. The snow under canopy is least important for dense forests where little light penetrates the canopy, but becomes important for short vegetation because most understories such as grass, moss,

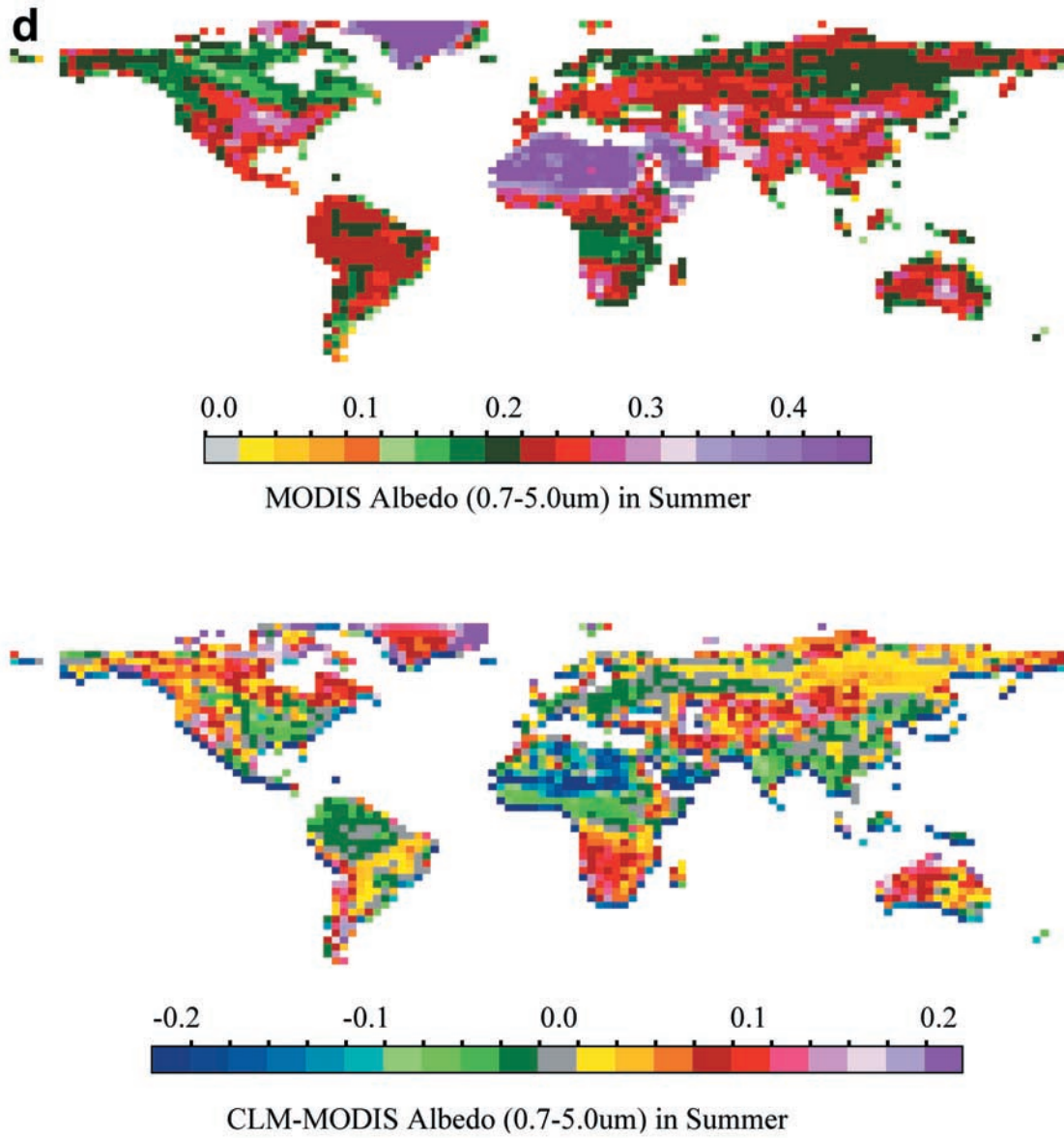


Figure 4. (continued)

Table 4. Area Average Winter Albedos of MODIS and CLM Over Grids Beyond 50°N With the Purity for the Dominant Land Cover Type Greater Than 60%

IGBP Landcover Type	Visible (0.3–0.7 μm)		Near-Infrared (0.7–5.0 μm)		CLM LSAI	Total Grid Number ^a
	MODIS ^b	CLM-MODIS	MODIS ^b	CLM-MODIS		
1	0.40 (0.42)	−0.13	0.31 (0.32)	0.00	2.0	68 (0.89)
3	0.44 (0.45)	−0.24	0.32 (0.32)	−0.01	1.3	29 (0.95)
5	0.37 (0.40)	−0.04	0.30 (0.31)	0.06	1.2	24 (0.85)
6	0.55 (0.63)	−0.20	0.36 (0.40)	−0.02	0.5	4 (0.93)
7	0.78 (0.78)	−0.30	0.47 (0.47)	−0.05	1.0	52 (1.00)
8	0.71 (0.71)	−0.34	0.43 (0.43)	−0.06	1.4	15 (1.00)
11	0.70 (0.70)	−0.28	0.44 (0.34)	−0.05	1.6	10 (0.99)
12	0.47 (0.57)	−0.13	0.34 (0.38)	0.02	0.4	27 (0.67)
14	0.29 (0.42)	−0.01	0.28 (0.32)	0.07	0.6	14 (0.73)
15	0.84 (0.84)	0.01	0.46 (0.46)	0.19	0.0	79 (1.00)
18	0.84 (0.84)	−0.13	0.47 (0.47)	0.09	0.2	89 (1.00)

^aValues in parenthesis represent percentage of snowy pixels to total pixels.

^bValues in parenthesis are averaged from snowy pixels only.

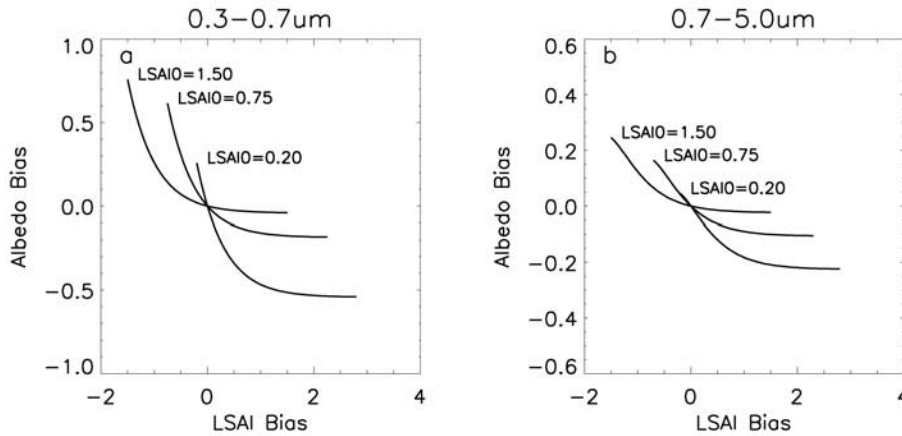


Figure 5. Albedo bias versus LSAI bias relationship simulated from equation (12) for vegetation with actual LSAI: 0.2, 0.75, and 1.5 and canopy albedos, $\alpha_c = 0.05$ in VIS and 0.23 in NIR, under underlying surface condition: snow, $\alpha_g = 0.85$ for VIS and 0.5 for NIR, SZA = 60°: (a) VIS and (b) NIR.

lichen, etc. can be covered by snow. The openings are implicit in the “bare” fraction. So possibly, the model needs to better represent openings, f_{scv} and f_{scs} . Currently, the openings are based on summer NDVI [Zeng et al., 2002] and presumably would not handle very well understories for short vegetation and increased gaps due to fall of leaves for dense forests in winter. CLM determines f_{scv} and f_{scs} by relating them to grid-averaged snow depth and surface roughness length (equations (2) and (3)). Such relation, however, should vary in terms of differences in topography, vegetation fraction and type, season, accumulation and melting curve (Yang et al., manuscript in preparation, 2003).

[41] Large biases can also occur if the model’s snow cover differs from reality, especially in middle latitudes

where snow cover is partial. For example, the biases in middle latitude grasslands/croplands in both Eurasia and North America are likely due to the model’s low snow cover fraction. In contrast, the largest biases are observed over most of western China and neighboring areas (30°–50°N, 75°–100°E), where CLM predicts that snow covers 40–100% of the model grids and thus gives VIS albedo of about 0.4–0.8 and NIR albedo of about 0.3–0.6. MODIS, in comparison, observes no or less snow for most of this area and has albedo values of around 0.2 for VIS and about 0.3 for NIR. Figure 9 illustrates seasonal variations of CLM and MODIS albedo for a model grid (40.5°N, 90.0°E) in this region. It is defined as 100% bare soil. CLM gives winter albedo of around 0.70 for VIS and 0.55 for NIR because

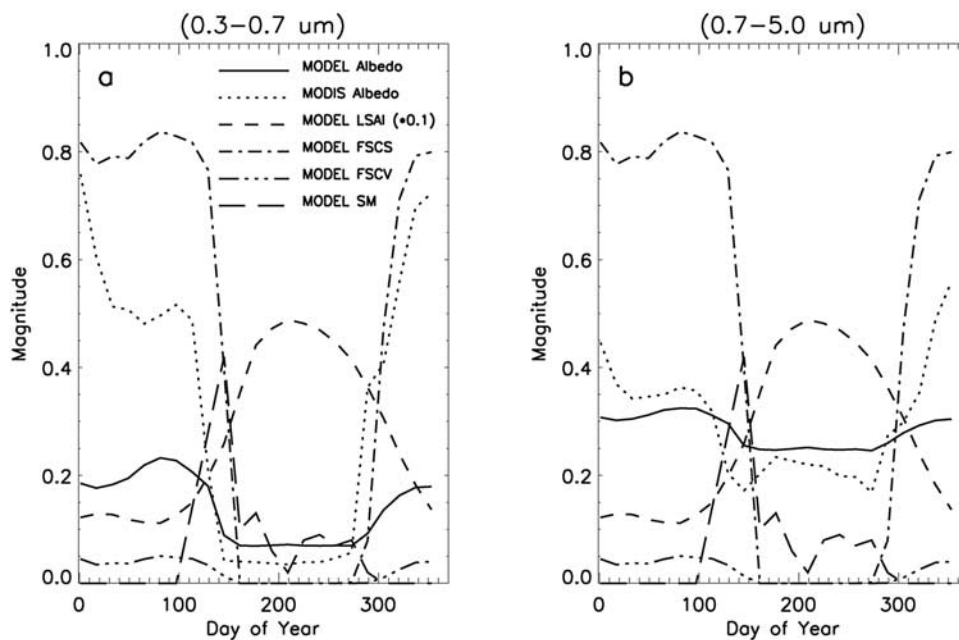


Figure 6. Seasonal variations of albedos from MODIS and CLM, together with fraction of snow covered soil (FSCS), fraction of snow covered vegetation (FSCV), soil moisture (SM), leaf and stem area index (LSAI) from CLM, for a grid located at 62.8°N, 106.9°W and consisting of 75% deciduous needleleaf forests, 12% woody savannas, and 13% bare soil: (a) VIS and (b) NIR.

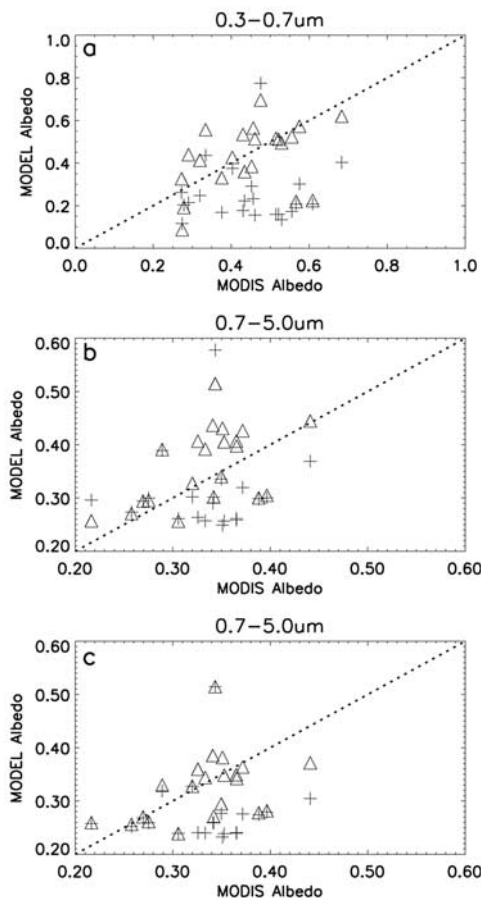


Figure 7. Relation between MODIS and CLM albedo beyond 50°N for evergreen needleleaf forests. Symbols “plus” and “triangle” refer to albedos before and after using the derived LSAI based on MODIS albedo, respectively. (a) VIS, (b) NIR, (c) as Figure 7b but setting CLM pure snow NIR albedo to the MODIS value of 0.49.

snow covers about 75% of the grid ($f_{sns} = 75\%$), while MODIS sees no snow and has albedo around 0.2 for VIS and 0.25 for NIR.

[42] The greater snow in the model than in the MODIS data probably results in higher model albedo by about 0.3–0.5. For example, model grids in the Chinese Taklimakan desert have elevations higher by up to 1–2 km than those from digital elevation maps [NGDC, 1988], resulting from the low-resolution GCM smoothing of the Tibetan Plateau. Higher elevation would have colder temperature and might generate more upward motion necessary for precipitation (rain or snow). In addition, MODIS tends to have snow-free albedos in regions with ephemeral snow since the MODIS albedo algorithm only uses the snowy pixel observations to make a retrieval if the majority of days in a 16-day period have been snow covered. Since the current MODIS data uses normalized snow difference indices (D. Hall et al., Algorithm Theoretical Basis Document (ATBD) for the MODIS snow-, lake ice- and sea ice-mapping algorithms, 1998, available at http://modis-land.gsfc.nasa.gov/pdfs/atbd_mod10.pdf) [Hall et al., 2002] to assess the presence of snow when a threshold value is exceeded, uncertainties in the snow detection may result in low confidence in MODIS

albedo retrievals. For example, this method may label dense vegetation partially underlain by snow as snow free and therefore increase its albedo by using the MODIS snow-free retrieval algorithm.

4.2.2. Soil Albedo

[43] On average, CLM gives VIS and NIR albedos over deserts and semideserts in North Africa and the Arabian peninsula that are lower by about 0.1, with some regions and seasons (Figure 4) lower by up to 0.2. Figure 10 shows seasonal variations of pure soil albedo for a grid in Sahara (18.1°N, 14.1°E). CLM albedos remain constant over most periods but drop by 0.05 in VIS and 0.1 in NIR due to increased soil moisture in summer (wet season). MODIS exhibits small variations around the year. The model albedo is lower by up to 0.12 in VIS and 0.2 in NIR.

[44] In contrast, over the Australian desert, CLM overestimates the albedo by about 0.06 in VIS and about 0.1 in NIR. Figure 11 displays seasonal variations of albedo for a grid in this region (20.9°S, 120.9°E). It consists of 74% bare soil and 24% of open shrublands. The model gives almost a constant LAI value around 0.5 for the shrublands. MODIS LAI varies between 0.3 and 0.4. A difference of 0.1 in LAI could contribute only 10% of the bare soil albedo, too small to explain the observed biases. Soil moisture mainly controls albedo variations in the model.

[45] The situation becomes complex in Chinese desert and semidesert regions. In general, the model gives a lower VIS albedo and a higher NIR albedo in snow-free seasons.

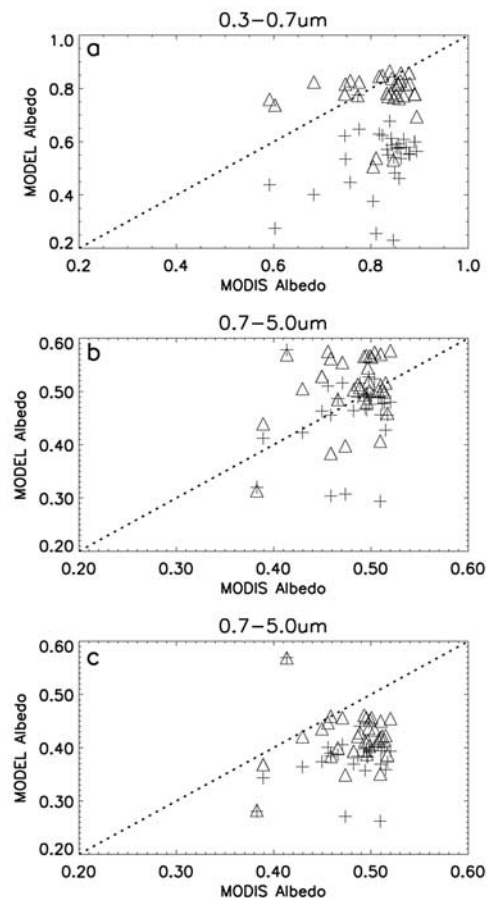


Figure 8. Same as Figure 7 but for open shrublands.

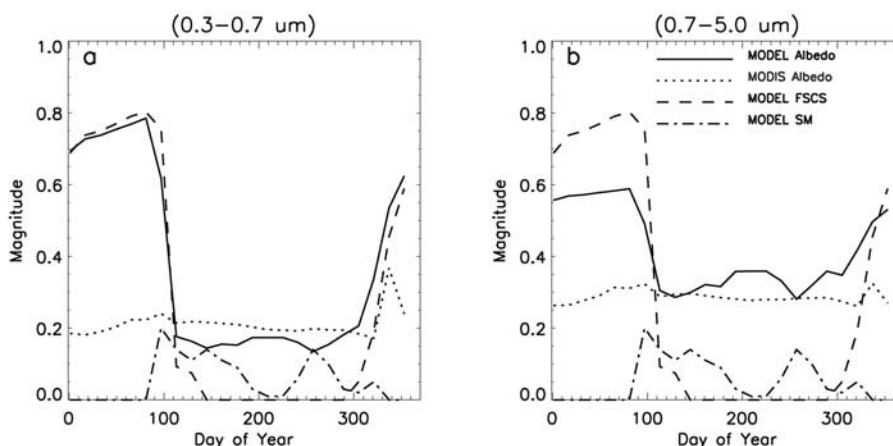


Figure 9. Seasonal variations of albedos from MODIS and CLM, together with fraction of snow covered soil (FSCS) and soil moisture (SM) from CLM, for a grid located at 40.5°N, 90.0°E and consisting of 100% bare soil: (a) VIS and (b) NIR.

This can be seen from the grid (Figure 9), which shows a low (high) bias of 0.05 in the VIS (NIR) albedo in summer.

[46] Apparently, the above biases differ in either direction, depending on differences in soil composition and wetness over different regions. They may be attributed to several factors, such as the simple representation of soil albedo in CLM, satellite data quality, variations of surface conditions, and limitations of narrow-to-broadband conversions in MODIS.

[47] Soil albedo varies widely, depending largely on the soil mineralogical composition and wetness. Considerable spatial variability in surface albedo over deserts and semi-deserts has been observed [Pinty *et al.*, 2000; Strugnell *et al.*, 2001; Tsvetinskaya *et al.*, 2002]. Soil albedo in CLM is based on limited observations and equation (4), as a function of soil color and moisture. It assumes that the ratio of NIR to VIS saturated albedo is 2 for each soil type (Table 2). This simple representation may capture major soil features, but lose some spatial and spectral information.

[48] MODIS albedos are generally higher than those derived from AVHRR [Strugnell *et al.*, 2001; Wei *et al.*,

2001]. They are believed to be more reliable due to more spectral bands and higher quality than other satellites like AVHRR. Some variations in MODIS albedo may be related to inadequate atmospheric corrections, especially for the effects of cloud and aerosol. The former should be largely removed by the intensive cloud clearing algorithms in the MODIS production, while the latter should be largely removed by the 16-day modeling used in MODIS and only be significant for those poorest quality albedos where either insufficient data are available or data are over extremely bright surfaces.

[49] Differences in soil moisture between the model and reality could be large and may account for some albedo differences, but probably not the observed systematic biases. Assuming that MODIS represents the reality of bare soil albedo, the seasonal variation for each grid could reflect the influence of varying SZA and soil moisture. For most grids, however, such variations are smaller than the observed biases.

[50] MODIS surface broadband albedos are derived from narrowband observations, requiring several levels of processing [Lucht *et al.*, 2000b; Liang, 2001; Liang *et al.*,

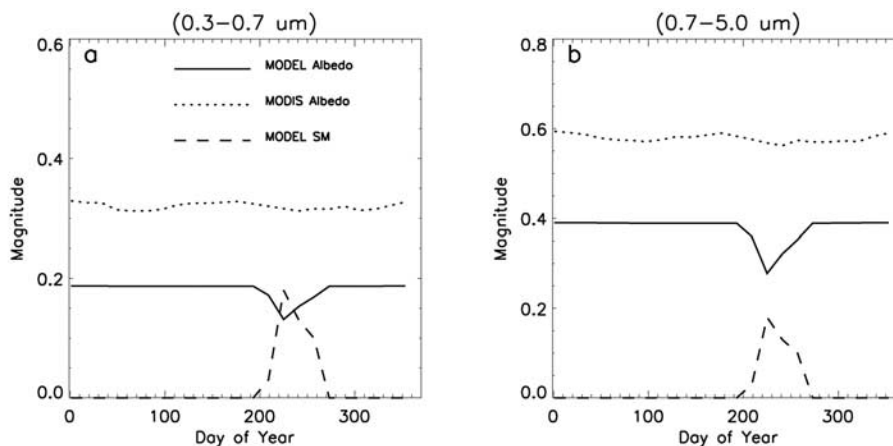


Figure 10. Seasonal variations of albedos from MODIS and CLM, together with soil moisture (SM) from CLM, for a grid located at 18.1°N, 14.2°E and consisting of 100% bare soil: (a) VIS and (b) NIR.

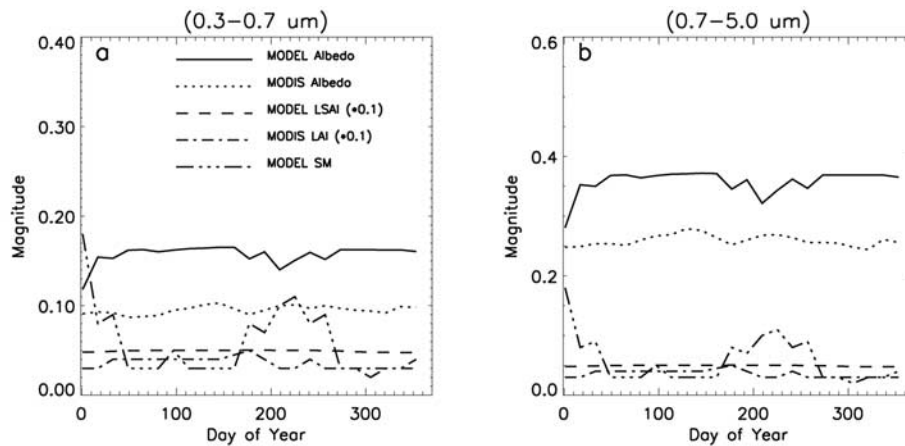


Figure 11. Seasonal variations of albedos from MODIS and CLM, together with soil moisture (SM) and leaf and stem area index (LSAI) from CLM and leaf area index (LAI) from MODIS, for a grid located at 20.9°S, 120.9°E and consisting of 74% bare soil and 24% open shrublands: (a) VIS and (b) NIR.

2002]. Errors could arise and accumulate at any step. Most narrow-to-broadband conversions are based on a limited number of surface reflectance spectra, either from field measurements or from model simulations. Soil and vegetation differ in detailed structure of spectral reflectance. So does soil with different colors and wetness over different regions. Measurements by *Ishiyama et al.* [1996] demonstrate significant differences in the soil spectral reflectance versus moisture content relationship, especially in NIR. Hence the soil reflectance spectra assumed by MODIS may differ from that appropriate for a given desert region and therefore the narrow-to-broadband conversion. As a result, the ratio of NIR to VIS albedo may be inaccurate. This is also true for CLM, which assumes that the ratio of NIR to VIS saturated soil albedo is always equal to 2. Figure 12 shows the ratios for MODIS and CLM in Sahara, Taklimakan, and the Australian desert. Only those grids with LAI less than 0.5 and with minimum albedo during wet seasons were selected. On average, MODIS varies from a ratio of 1.63 in the Taklimakan to 2.69 in the Australian desert. CLM has small spatial variations, with most values slightly larger than 2, the excess over 2 due to existence of some vegetation.

[51] Clearly, MODIS captures more spatial and seasonal variations than CLM and should be closer to reality. Observations in the Taklimakan desert [*Ishiyama et al.*, 1996] give an average albedo of 0.21 for 0.3–0.7 μm, which is comparable with MODIS, but larger than that of the model (Figure 9a). Ground-based measurements [*Lucht et al.*, 2000b] over some validation sites suggest an accuracy of ± 0.03 for MODIS-derived albedos.

4.2.3. Vegetation Albedo

[52] The small difference between canopy and its underlying soil albedo makes the comparison between MODIS and model albedos complex because the biases could result from either vegetation or its underlying soil or both. Figure 13 shows the simulated albedo bias versus LSAI bias relation for vegetation for three LSAI values (LSAIO = 1, 3, and 6) under two situations; the underlying soil is either darker or brighter than the canopy. Two extreme cases were used, one (the other) is the darkest (brightest) in Table 2a, $\alpha_g = 0.05$ (0.23) for VIS and 0.1 (0.46) for NIR. Other

parameters include: (1) SZA = 10°; and (2) canopy albedo, $\alpha_c = 0.14$ for VIS and 0.32 for NIR.

[53] For dense vegetation (LSAIO = 6), albedo is insensitive to the LSAI bias. Consequently, VIS albedo biases over most dense forests in the Amazon, boreal forests, southeast USA, and central Africa may mainly result from the slightly higher prescribed canopy albedos as discussed in section 3, while the small NIR albedo biases may be due to lower prescribed canopy albedo for some vegetation types, uncertainties in MODIS albedo, or soil albedo (about 10% soil). Figure 14 shows seasonal variations of CLM and MODIS albedo for a grid in the Amazon (4.2°S, 75.9°W). Evergreen broadleaf trees and bare soil cover 93 and 7% of the grid, respectively. To avoid cloud contamination, we focus on dry season albedo only. The difference in both VIS and NIR is very small, about 0.02. Soil moisture shows large variations but has a small effect due to the small fraction of exposed soil.

[54] For short vegetation and LSAI in the range of 1–3, the LSAI bias can affect albedo in either direction, depending on whether the underlying soil is brighter or darker than the canopy, and can be largest when LSAI is smallest. For very sparsely vegetated regions, soil dominates albedo variations and any contribution from the LSAI bias is small. For example, lower albedos are seen in the southern border of Sahara although there are higher LSAIs in the region compared to MODIS data. For regions with more vegetation in western China, Australian, and south Africa, where shrub, savanna, and grass dominate and the model gives higher LSAI than MODIS, CLM overestimates VIS albedos by up to 0.05 and NIR albedos by up to 0.1, resulting from the model having either higher canopy albedo or underestimated soil albedo (Figure 13). Of model grids with biases greater than 0.1 in NIR and 0.03 in VIS between 50°S and 50°N, 57 and 39% contain open shrublands and grasslands, respectively, more than any other vegetation type.

[55] To illustrate this further, we selected a grid (Figure 15) in South America (7.0°S, 39.4°W) with the largest fraction of shrublands (66% open shrublands, 21% closed shrublands, and 13% bare soil) defined by the model. MODIS LAI shows a significant seasonal variation from 0.5 to 4,

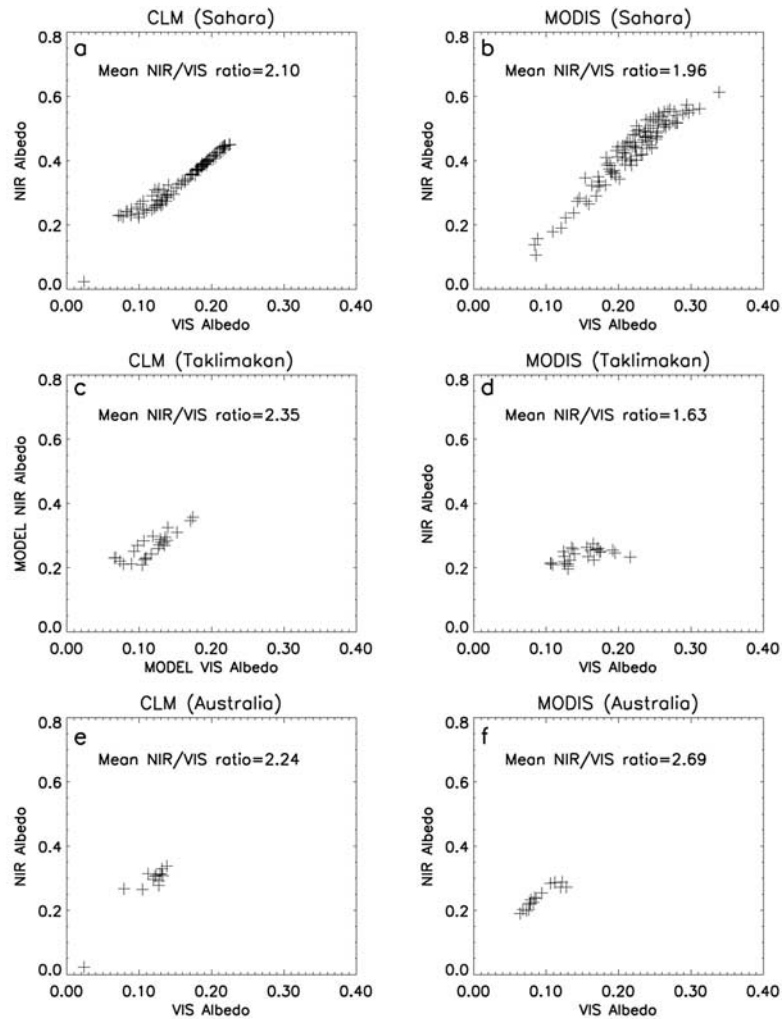


Figure 12. Relation between VIS and NIR albedos for those desert and semidesert grids with LAI less than 0.5 and with minimum albedo during wet seasons: (a) CLM in Sahara, (b) MODIS in Sahara, (c) CLM in Taklimakan, (d) MODIS in Taklimakan, (e) CLM in the Australian desert, and (f) MODIS in the Australian desert.

making it a perfect example of how albedo changes as LAI changes, while CLM exhibits a smaller variation, resulting in a higher LAI by up to 1.2 in July–December and a lower LAI by up to 1.8 in March–May. The canopy and soil albedos are comparable in the model and thus the albedo varies little through the year although the model LSAI shows a strong seasonality. The model VIS albedo shows the largest bias (higher by up to 0.05 than MODIS) in March to May when vegetation peaks mainly due to the higher prescribed model canopy albedo (Figure 1). From the MODIS NIR albedo, we can infer that the underlying soil is darker than canopy in NIR (Figure 15b) since the maximum albedo (when LAI peaks) is larger than the minimum value (when LAI minimizes). The largest NIR albedo bias in July–December when vegetation is minimum may be mainly due to the higher model LSAI (Figure 13b).

[56] The simplified two-stream scheme used in CLM may also attribute to part of the albedo biases due to its neglect of multiple scattering. It can be an exact solution for a homogeneous canopy but may be unrealistic in terms of dependence on SZA since it does not include the geometric

effects of individual plant elements and their shadowing of other plants and underlying surfaces. Such shadowing acts to reduce or invert the strong increase of albedo with sun angle seen in the homogeneous models [Dickinson, 1983].

5. Discussion and Conclusions

[57] This paper compares MODIS albedos with those from the CLM [Zeng *et al.*, 2002; Dai *et al.*, 2003]. The MODIS albedo data in 2001 are used to determine seasonal, spatial, and land cover dependence of albedo at 1 km resolution, and to investigate differences of albedos between MODIS and CLM at about $2.8^\circ \times 2.8^\circ$ resolution. The objective is to use this information to improve parameterization of albedo in CLM.

[58] Analyses of MODIS 1 km albedo data indicate albedo dependence on vegetation type is smaller than that on snow and soil. VIS albedos are typically about 0.03 for dense forests and about 0.05–0.1 for short vegetation.

[59] Snow significantly increases albedo and causes the largest temporal and spatial variations, especially in the

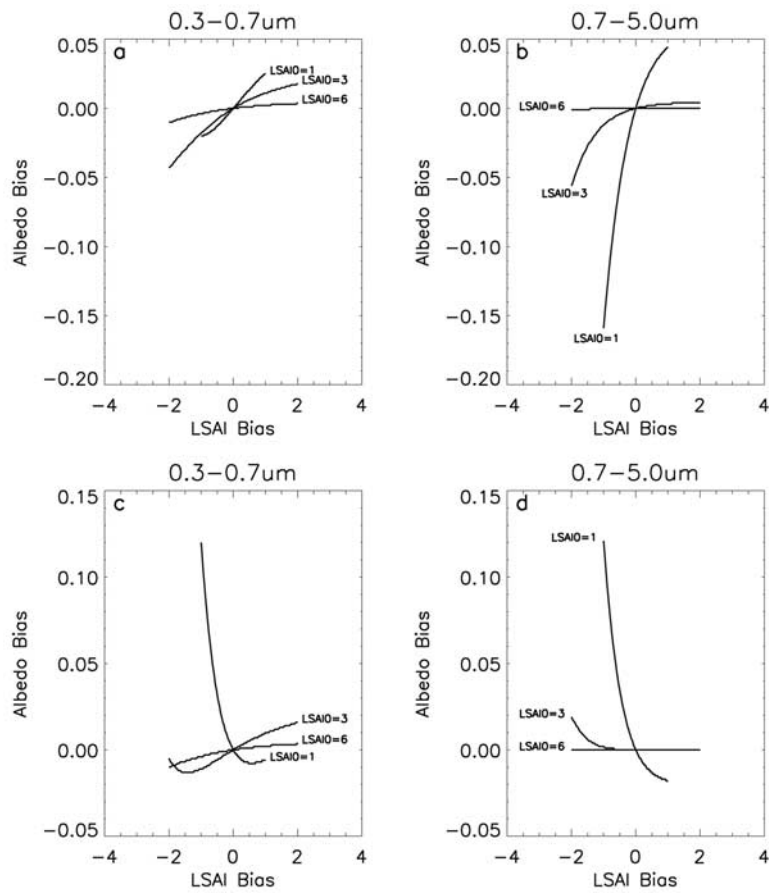


Figure 13. Albedo bias versus LSAI bias relationship simulated from equation (12) for vegetation with actual LSAI: 1, 3, and 6 and canopy albedos, $\alpha_c = 0.14$ in VIS and 0.32 in NIR, under two underlying surface conditions at $\text{SZA} = 10^\circ$: (1) $\alpha_g = 0.05$ for VIS and 0.23 for NIR; and (2) $\alpha_g = 0.23$ for VIS and 0.46 for NIR. (a) VIS and (b) NIR for the dark surface (1), and (c) VIS and (d) NIR for the bright surface (2).

visible (VIS, 0.3–0.7 μm). CLM gives winter albedos in the presence of snow that are lower by up to 0.4–0.5 than MODIS observations in northern high latitudes, mainly due to its overestimation of leaf and stem area index. Since snow has much higher albedo than most other natural

surfaces (e.g., 60–80% versus 10–30%), higher leaf and stem indexes decrease albedo of snow covered surfaces.

[60] The presence of snow adds complexity and brings greater uncertainty to surface albedo characterizations in the model. Our analysis indicates that model factors that drive

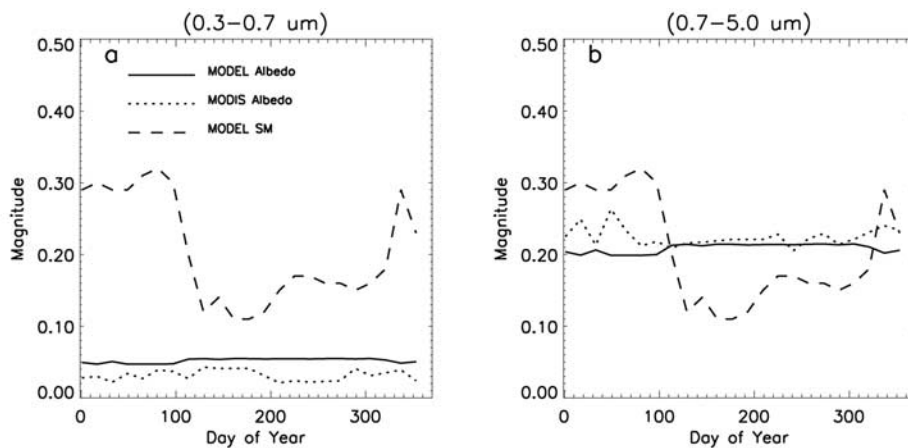


Figure 14. Same as Figure 10 but for a grid located at 4.2°S, 75.9°W and consisting of 93% evergreen broadleaf forests and 7% bare soil: (a) VIS and (b) NIR.

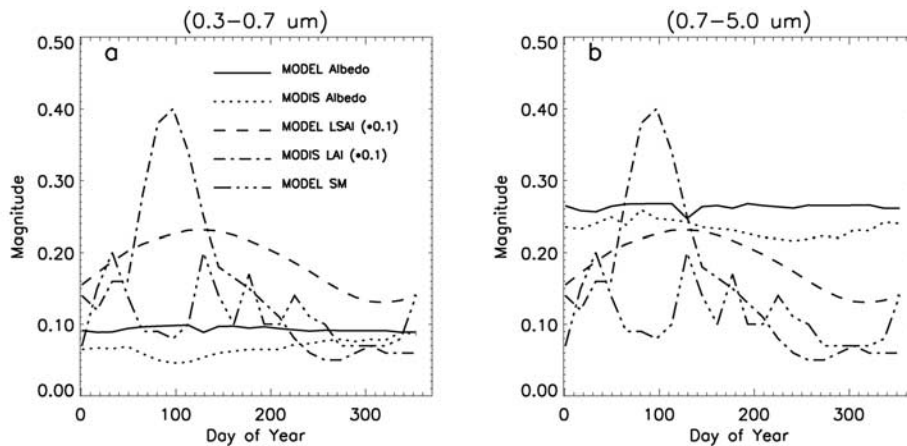


Figure 15. Same as Figure 11 but for a grid located at 7.0°S, 39.4°W and consisting of 66% open shrublands, 21% closed shrublands: (a) VIS and (b) NIR.

discrepancies with MODIS are (1) shading by the winter LAI and SAI, (2) inaccuracy in specification of fractional vegetation cover, and (3) inaccuracy in determining fractions of surface covered or not covered by snow. The MODIS albedo algorithm uses either snow-free or snow-present scenes to retrieve albedo, depending on which occurs more often over the 16-day period. This limits its application in the models, particularly under situations of snow-vegetation mixtures and ephemeral snow cover.

[61] Our study also highlights the role of SAI (stems and dead leaves) used in CLM to represent the effects of nongreen canopy surfaces. The model requires a prescribed constant canopy albedo for dense canopy in its radiation scheme but this value depends on the same leaf and stem single-scattering albedo. The SAI has very limited photosynthesis and thus should have very different single-scattering albedos from those of green leaves [Asner, 1998]. The equal treatment of SAI and LAI in the model makes the contribution of SAI to albedo much larger than that of LAI in winter. This may be inappropriate and the role of SAI in the parameterizations needs to be reformulated. A weighted single-scattering albedo may help capture the spectral differences between stem and leaf. In addition, SAI in CLM includes both stem and dead leaves and the latter might affect radiation between canopy and underlying soil but should not be considered when they are buried by snow.

[62] MODIS and CLM differ considerably in soil albedo over desert and semidesert regions, especially in the near-infrared (0.7–5.0 μm), with the model lower by about 0.1 over the Sahara. Soil albedo varies spatially and seasonally, depending largely on the soil mineralogical composition and wetness. The simple representation of CLM albedo, based on limited observations, may capture major soil features but not all the spatial and spectral information seen in MODIS. The albedo biases differ in either direction over different regions. Although there may be some uncertainties associated with satellite data quality, variations of surface conditions, and limitations of narrow-to-broadband conversions, MODIS albedos may be closer to reality than those of the model, as they are consistent with ground observations [Ishiyama et al., 1996; Lucht et al., 2000b; Liang et al., 2002]. Therefore the model needs to better represent spatial variability in soil albedo.

[63] Dense forests in the Amazon, boreal forests, south-east USA, and central Africa are insensitive to LAI biases. Their albedo biases of about 0.02–0.04 may result from prescribed slightly higher VIS (lower NIR) canopy albedos or uncertainties in MODIS albedo. For short vegetation, an LAI bias can affect albedo in either direction, depending on the magnitude and direction of the difference between canopy and its underlying soil albedo. Albedos are more sensitive to LAI bias in NIR than in VIS. Most sparsely vegetated regions in western China, Australia, and South Africa, where the LAIs are generally overestimated, have a high bias of 0.02–0.1, due to either the higher prescribed canopy albedo or underestimated soil albedos.

[64] **Acknowledgments.** This work was funded by the NASA EOS/IDS Program (NAG5-8880).

References

- Asner, G. P., Biophysical and biochemical sources of variability in canopy reflectance, *Remote Sens. Environ.*, 64, 234–253, 1998.
- Bonan, G. B., *A Land Surface Model (LSM Version 1.0) for Ecological, Hydrological, and Atmospheric Studies: Technical Descriptions and User Guide*, Tech. Note NCARTN-417+STR, 150 pp., Natl. Cent. of Atmos. Res., Boulder, Colo., 1996.
- Bonan, G. B., The land surface climatology of the NCAR land surface model (LSM 1.0) coupled to the NCAR Community Climate Model (CCM3), *J. Clim.*, 11, 1307–1326, 1998.
- Buermann, B., J. Dong, X. Zeng, R. B. Myneni, and R. E. Dickinson, Evaluation of the utility of satellite-based vegetation leaf area index data for climate simulations, *J. Clim.*, 14, 3536–3550, 2001.
- Dai, Y., et al., The common Land Model (CLM) version 1.0, *Bull. Am. Meteorol. Soc.*, in press, 2003.
- Dickinson, R. E., Land surface processes and climate-surface albedos and energy balance, *Adv. Geophys.*, 25, 305–353, 1983.
- Dickinson, R. E., and A. Henderson-Seller, Modeling tropical deforestation: A study of GCM land surface parameterizations, *Q.J.R. Meteorol. Soc.*, 114, 439–462, 1988.
- Dickinson, R. E., A. Henderson-Seller, and P. J. Kennedy, *Biosphere-Atmosphere Transfer Scheme (BATS) Version 1e as Coupled to the NCAR Community Model*, Tech. Note NCAR/TN-387+STR, 72 pp., Natl. Cent. of Atmos. Res., Boulder, Colo., 1993.
- Friedl, M. A., et al., Global land cover from MODIS: Algorithms and early results, *Remote Sens. Environ.*, 83, 287–302, 2002.
- Gutman, G. G., On the use of long-term global data of land reflectances and vegetation indices derived from the advanced very high resolution radiometer, *J. Geophys. Res.*, 104, 6241–6255, 1999.
- Hahmann, A. N., and R. Dickinson, CCM2-BATS model over tropical South America: Application to tropical deforestation, *J. Clim.*, 10, 1944–1964, 1997.
- Hall, D., G. Riggs, V. Salomonson, N. DiGirolamo, and K. Bayr, MODIS snow-cover products, *Remote Sens. Environ.*, 83, 181–194, 2002.

- Henderson-Sellers, A., and M. F. Wilson, Surface albedo data for climate modeling, *Rev. Geophys. Space Phys.*, 21, 1743–1778, 1983.
- Intergovernmental Panel on Climate Change, *Climate Change 2001: The Scientific Basis*, edited by J. T. Houghton et al., Cambridge Univ. Press, New York, 2002.
- Ishiyama, T., K. Tsuchiya, and S. Sugihara, Ground surface features of the Taklimakan desert, *Adv. Space Res.*, 17(8), 841–848, 1996.
- Jin, Y., C. B. Schaaf, F. Gao, X. Li, A. H. Strahler, X. Zeng, and R. E. Dickinson, How does snow impact the albedo of vegetated land surfaces as analyzed with MODIS data?, *Geophys. Res. Lett.*, 29(10), 1374, doi:10.1029/2001GL014132, 2002.
- Kiehl, J., J. Hack, G. B. Bonan, B. Bonville, D. L. Williamson, and P. J. Rasch, The national center for atmospheric research community climate model: CCM3, *J. Clim.*, 11, 1131–1149, 1998.
- Liang, S., Narrowband to broadband conversion of land surface albedo, I, Algorithms, *Remote Sens. Environ.*, 76, 213–238, 2001.
- Liang, S., A. H. Strahler, and C. Walthall, Retrieval of land surface albedo from satellite observations: A simulation study, *J. Appl. Meteorol.*, 38, 712–725, 1999.
- Liang, S., C. Shuey, A. Russ, H. Fang, M. Chen, C. Walthall, and C. Daughtry, Narrowband to broadband conversions of land surface albedo, II, Validation, *Remote Sens. Environ.*, 84, 25–41, 2002.
- Lucht, W., C. B. Schaaf, and A. H. Strahler, An algorithm for the retrieval of albedo from space using semiempirical BRDF models, *IEEE Trans. Geosci. Remote Sens.*, 38, 977–998, 2000a.
- Lucht, W., A. H. Hyman, A. H. Strahler, M. J. Barnsley, P. Hobson, and J.-P. Muller, A comparison of satellite-derived spectral albedos to ground-based broadband albedo measurements modeled to satellite spatial scale for a semi-desert landscape, *Remote Sens. Environ.*, 74, 85–98, 2000b.
- Myneni, R. B., et al., Global products of vegetation leaf area and fraction absorbed PAR from year one of MODIS data, *Remote Sens. Environ.*, 83, 214–231, 2002.
- NGDC, Data Announcement 88-MGG-02: Digital Relief of the Surface of the Earth, NOAA, Natl. Geophys. Data Cent., Boulder, Colo., 1988.
- Pinty, B., F. Roveda, M. M. Verstraete, N. Gobron, Y. Govaerts, J. V. Martonchik, D. J. Diner, and R. A. Kahn, Surface albedo retrieval from Meteosat 2, Applications, *J. Geophys. Res.*, 105, 18,099–18,112, 2000.
- Privette, J. L., T. F. Eck, and D. W. Deering, Estimating spectral albedo and nadir reflectance through inversion of simple BRDF models with AVHRR/MODIS-like data, *J. Geophys. Res.*, 102, 29,529–29,542, 1997.
- Robock, A., Ice and snow feedbacks and the latitudinal and seasonal distribution of climate sensitivity, *J. Atmos. Sci.*, 40, 986–997, 1983.
- Schaaf, C. B., et al., First operational BRDF, albedo, and nadir reflectance products from MODIS, *Remote Sens. Environ.*, 83, 135–148, 2002.
- Sellers, P. J., S. O. Los, C. J. Tucker, C. O. Justice, D. A. Dazlich, C. J. Collatz, and D. A. Randall, A revised land surface parameterization (SiB2) for atmospheric GCMs, part II, The generation of global fields of terrestrial biospheric parameters from satellite data, *J. Clim.*, 9, 706–737, 1996.
- Sellers, P. J., et al., Modeling the exchanges of energy, water and carbon between the continents and the atmosphere, *Science*, 275, 502–509, 1997.
- Strugnell, N. C., W. Lucht, and C. Schaaf, A global albedo data set derived from AVHRR data for use in climate simulations, *Geophys. Res. Lett.*, 28, 191–194, 2001.
- Tsvetinskaya, E. A., C. B. Schaaf, F. Gao, A. H. Strahler, R. E. Dickinson, X. Zeng, and W. Lucht, Relating MODIS-derived surface albedo to soils and rock types over northern Africa and the Arabian peninsula, *Geophys. Res. Lett.*, 29(9), 1353, doi:10.1029/2001GL014096, 2002.
- Wei, X., A. N. Hahmann, R. E. Dickinson, Z.-L. Yang, X. Zeng, K. J. Schaudt, C. B. Schaaf, and N. Strugnell, Comparison of albedos computed by land surface models and evaluation against remotely sensed data, *J. Geophys. Res.*, 106, 20,687–20,702, 2001.
- Wiscombe, W., and S. G. Warren, A model for the spectral albedo of snow, I, Pure snow, *J. Atmos. Sci.*, 37, 2712–2733, 1980.
- Xue, Y., and J. Shukla, The influence of land surface properties on Sahel climate, part I, Desertification, *J. Clim.*, 6, 2232–2245, 1993.
- Xue, Y., K.-N. Lion, and A. Kasahara, Investigation of biogeophysical feedback on African climate using a two dimensional model, *J. Clim.*, 3, 337–352, 1990.
- Zeng, X., M. Shaikh, Y. Dai, R. E. Dickinson, and R. B. Myneni, Coupling of the common land model to the NCAR community climate model, *J. Clim.*, 14, 1832–1854, 2002.

Y. Dai, R. E. Dickinson, M. Shaikh, Y. Tian, W. Wu, H. Yu, and L. Zhou, School of Earth and Atmospheric Sciences, Georgia Institute of Technology, 311 Ferst Drive, Atlanta, GA 30332, USA. (dai@eas.gatech.edu; robted@eas.gatech.edu; shaikh@flux.eas.gatech.edu; ytian@eas.gatech.edu; wwu@eas.gatech.edu; hyu@eas.gatech.edu; lmzhou@eas.gatech.edu)

F. Gao, Y. Jin, R. B. Myneni, C. B. Schaaf, and A. Strahler, Department of Geography, Boston University, Boston, MA 02215, USA. (fgao@bu.edu; yfj@bu.edu; myneni@bu.edu; schAAF@bu.edu; alan@bu.edu)

Z.-L. Yang, Department of Geological Sciences, University of Texas at Austin, Austin, TX 78712, USA. (liang@mail.utexas.edu)

X. Zeng, Institute of Atmospheric Physics, University of Arizona, Tucson, AZ 85721, USA. (xubin@gogo.atmo.arizona.edu)